A RAPID ESTIMATION OF MOMENT MAGNITUDE M_W FOR THE OCTOBER 23, 2011 VAN EARTHQUAKE USING STRONG-MOTION RECORDS

by

İrfan Kılıç

B.S., Physics, Boğaziçi University, 2008

Submitted to the Kandilli Observatory and Earthquake Research

Institute in partial fulfillment of the requirements for the degree of

Master of Science

Graduate Program in Geophysics

Boğaziçi University

2014

ACKNOWLEDGEMENTS

Firstly I would like to thank my supervisor Prof. Dr. Nurcan Meral Özel who suggested me this subject for my M.S thesis and encouraged me at every point along the way during my study. I also would like to thank Assist. Prof. A. Özgün Konca with whom I made important discussions on the subject of this study. I benefited much from his valuable suggestions. I would like to thank all colleagues in KOERI especially Zeynep Yılmaz who helped me in technical issues.Finally I would like to thank my friends Hatip Kabak and Yüce Aydoğan who motivated me much during this work.

ABSTRACT

A RAPID ESTIMATION OF MOMENT MAGNITUDE M_W FOR THE OCTOBER 23, 2011 VAN EARTHQUAKE USING STRONG-MOTION RECORDS

It is well known that the Richter scale (local magnitude scale, M_L) based on the measurement of the amplitude in a narrow- band time domain saturates for large crustal earthquakes, and the possibility of observing clipping on seismograms is high. Therefore it is insufficient to use the local magnitude for reliable magnitude estimation. A typical example of this situation is confronted in case of the October 23, 2011 Van Earthquake (M_L 6.6 vs M_W 7.2) . Here M_W is the moment magnitude obtained from the far-field displacement spectrum of body waves. On the other hand, a better match is expected in the range of $3 < M_L < 7$ because in this range the empirical relation between seismic moment M_0 and M_L is almost the same with the relation between M_0 and M_W (Thatcher and Hanks, 1973; Hanks and Kanamori, 1979). Hence, there is a1234E need to find a way for the determination of M_W from near-field records too.The aim of this study is to determine moment magnitude of earthquakes very soon after occurrence, before any source or focal mechanism inversions have been performed. In this respect (Delouis *et al*., 2009) proposed the MWSYNTH method. In this method, observed displacement spectra are compared with synthetic spectra computed for a variety of finite dimension source models scaled with M_W.

In this study we have tried to obtain a rapid estimation of Mw for the October 23, 2011 Van Earthquake from the strong-motion records in the epicentral distances about 120 km using MWSYNTH method. Using strong motion records of only two stations we obtained an agreeable estimation of moment magnitude M_W=6.9. The result may be improved (approach more seriously to the reference moment magnitude M_W ref=7.15) by doing computation for more stations and it is foreseen that a correct recovery

of M_W for the Van Earthquake within about 100 sec after origin time (recording+computing time) will be possible if the procedure is automated.

ÖZET

KUVVETLİ YER HAREKETİ KAYITLARINDAN YARARLANILARAK 23 EKİM 2011 VAN DEPREMİ'NİN MOMENT BÜYÜKLÜĞÜNÜN HIZLI HESABI

Büyük depremler meydana geldiğinde, dar-bant zaman aralığındaki genlik ölçümlerine dayanan Richter ölçeği (lokal büyüklük ölçeği, M_L) satürasyona uğrar. Ayrıca sismogramlarda kırpılma gözlenilmesi ihtimali yüksektir. Bu yüzden güvenilir bir büyüklük hesabı için, lokal büyüklük ölçeğinin kullanılması yetersiz olmaktadır. 23 Ekim, 2011 Van Depremi'nde de bu durumun tipik bir örneği ile karşılaşılmış olup, depremin lokal büyüklüğü ile moment büyüklüğünün oldukça farklı olduğu anlaşılmıştır (M_L 6.6 , M_W 7.2). M_W, uzak mesafelerdeki cisim dalgalarının deplasman spektrumlarından elde edilen moment büyüklüğünü göstermektedir. Buna karşın, $3 < M_L < 7$ aralığında daha iyi bir uyum beklenilebilir. Bunun nedeni ise, M_L bu aralıkta iken, sismik moment M_0 ile M_L arasındaki ampirik ilişkinin neredeyse M_0 ile M_W arasındaki ilişkiyle aynı olmasıdır (Thatcher ve Hanks, 1973; Hanks ve Kanamori, 1979). Bunlardan yola çıkarak, moment büyüklüğünün yakın mesafelerdeki kayıtlardan yararlanarak hesaplamanın da bir yolunun bulunması gerektiği anlaşılmaktadır. Bu tezin amacı, hiçbir kaynak ya da fay mekanizması ters çözüm dönüşümü uygulanmadan önce, depremin moment büyüklüğünü hızlı olarak belirleyebilmektir. Bu amaçla (Delouis *et al*., 2009) tarafından MWSYNTH yöntemi önerilmiştir. Bu yöntemle, gerçek verilerin deplasman spektrumlarının düşük frekanslardaki genliği ile sismik momentle ölçekli kinematik kırık modelleri kullanılarak hesaplanmış olan sentetik kayıtların spektrum genlikleri kıyaslanmaktadır.

Bu çalışmada, MWSYNTH metodunu kullanarak 23 Ekim 2011 Van Depremi'nin moment büyüklüğü merkezüssüne 120 km uzaklıklarındaki iki istasyonun kuvvetli yer hareketi kayıtları kullanılarak M_W=6.9 olarak belirlenmiştir. Daha çok istasyon için hesaplama yapılırsa, sonuç referans alınan değere (M_W ref=7.15) daha çok yaklaşabilir. Bu çalışmada uygulanan hesaplama işleminin otomatik hale getirilmesi ile depremin oluş

zamanından itibaren yaklaşık 100s (kayıt zamanı+hesaplama zamanı) içinde depremin moment büyüklüğünün yakın alan kuvvetli yer hareketi kayıtları kullanılarak hızlıca belirlenebilmesinin mümkün olacağı öngörülmektedir.

TABLE OF CONTENTS

LIST OF FIGURES

LIST OF TABLES

LIST OF SYMBOLS / ABBREVIATIONS

l	Rupture length
m_b	Body wave magnitude
M_L	Local magnitude
M_S	Surface wave magnitude
M_W	Moment magnitude
M_0	Sismic moment
P	Primary wave
S	Secondary wave
S_L	Spectral level (maximum level of displacement spectrum at low frequencies)
Δu	Dislocation (slip)
μ	Rigidity
w	Rupture width
W	Shortest time window allowing theoretical computation of M_W
90w	Time window ending 90 sec after the origin time
E-W	East-West component of a seismogram
N-S	North-South component of a seismogram
U-D	Up-Down (vertical) component of a seismogram
MWSYNTH	Name of the method
AFAD	Afet ve Acil Durum Yönetimi Başkanlığı
KOERI	Kandilli Observatory and Earthquake Research Institute
NEMC	National Earthquake Monitoring Centre
USGS	The United States Geological Survey
NAF	North Anatolian Fault
EAF	East Anatolian Fault
BS	Bitlis Suture
KbF	Kavakbaşı Fault
ÇDFZ	Çobandele Fault zone
KF	Kağızman Fault

TF	Tutak Fault
BGF	Balık Lake Fault

1. INTRODUCTION

The destructive Van Earthquake in 2011 hit at 13:41 local time (10:41 GMT) on October 23, 2011. It was an event with M_L 6.6 and Mw 7.2 (KOERI) at a depth of 5 km with epicenter located near Tabanlı village, in the northeast of the city. Focal mechanism solutions revealed an East–West oriented thrust fault mechanism.The strike, dip and rake angles are 255°, 50° and 73° respectively (USGS). Estimates of the moment magnitude range from Mw 7.1 to Mw 7.3 and those of depth from 5 to 20 km from different institutions (Figure 1.1). The area of Lake Van and its surroundings belongs to the East Anatolian tectonic region of Turkey. It is well known that the seismicity of this region is dominated by the Bitlis Suture Zone and Zagros fold and thrust belt. On a broad scale, the region near the earthquake is under the effect of the collision of the Arabian Plate and Eurasian Plate**.** The fault motion suggests that the event belongs to the broad Bitlis Zagros Fault Zone (Örgülü *et al.*, 2003).

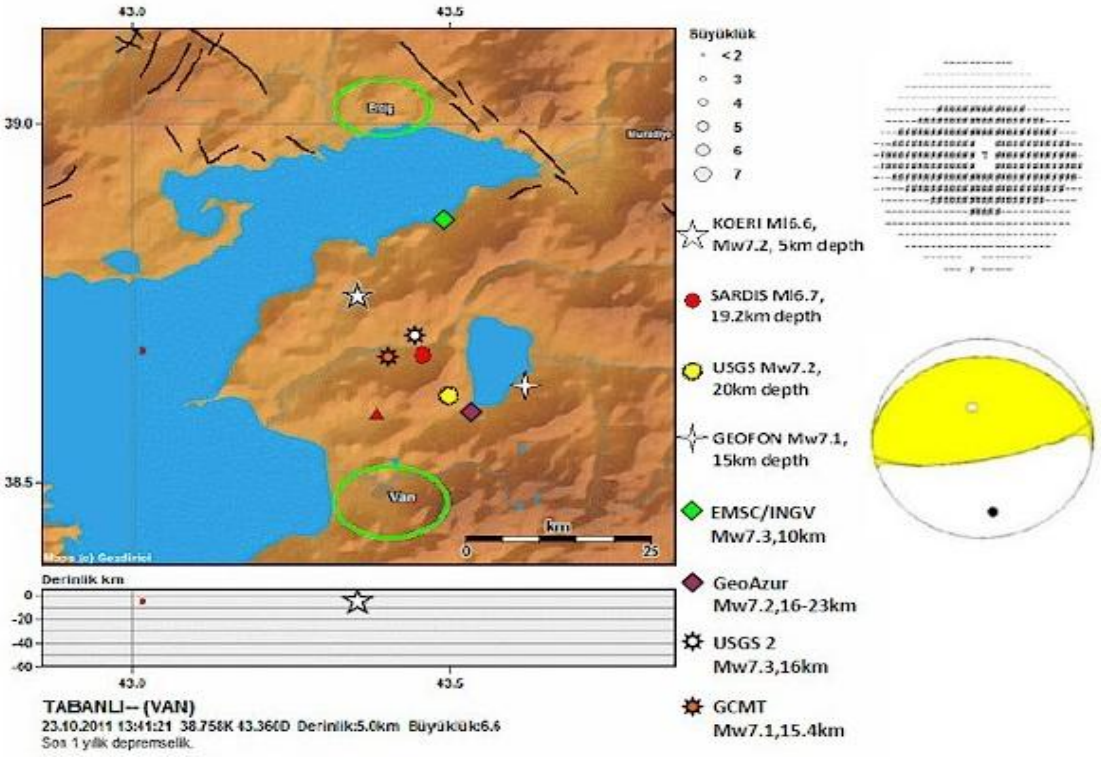

Figure 1.1. Hypocenters as determined from various agencies as compared to the large population areas of Van and Erciş (base picture courtesy of KOERI).

The aim of this study is to recover the apparent discrepancy between M_L and M_W. In order to do this, we computed M_W in place of M_L by using strong-motion records. The real-time determination of M_W based on near- field records is a challenge in seismology. Kanamori (1977) defined M_W as a logarithmic measure of seismic moment which can be obtained from displacement spectrum of body waves in far-field where point source approximation can be made safely and the seismic moment can be analytically related to the spectral amplitude (Brune, 1970,1971). However the relation between the seismic moment and the spectrum of near-field seismograms is not simple for large earthquakes because waves do not arrive (Figure 1.2) separately which result in complex radiation patterns and geometrical expansion factors (Aki and Richards, 1980).

In this respect strong-motion records are very important since they can preserve original earthquake information in the near-field. Studies on strong-motion records showed that magnitude may be obtained from the initial part of the P wave (Allen and Kanamori, 2003; Wu and Kanamori, 2008; Wu and Zhao, 2006; Zollo *et al*., 2006). Initiated with these studies (Delouis *et al*., 2009) developed the MWSYNTH method in which observed displacement spectra are compared with synthetic spectra computed for a variety of finite dimension source models in the near-field domain. The application of the MWSYNTH method to the October 23, 2011 Van Earthquake is presented in this thesis.We choosed two suitable stations from the strong-motion network of Turkey and for generating synthetic seismograms we used the FK method (Zhu, 2011) for a 1D layered velocity model adapted to the study area.For rupture time and rise time values associated to magnitude which is needed in synthetic seismogram formation we benefited from Heaton (1990) and Sato (1989). Spectra are calculated for different time windows so as to get early estimates of the moment magnitude and to analyze how the length of time window affects magnitude values.

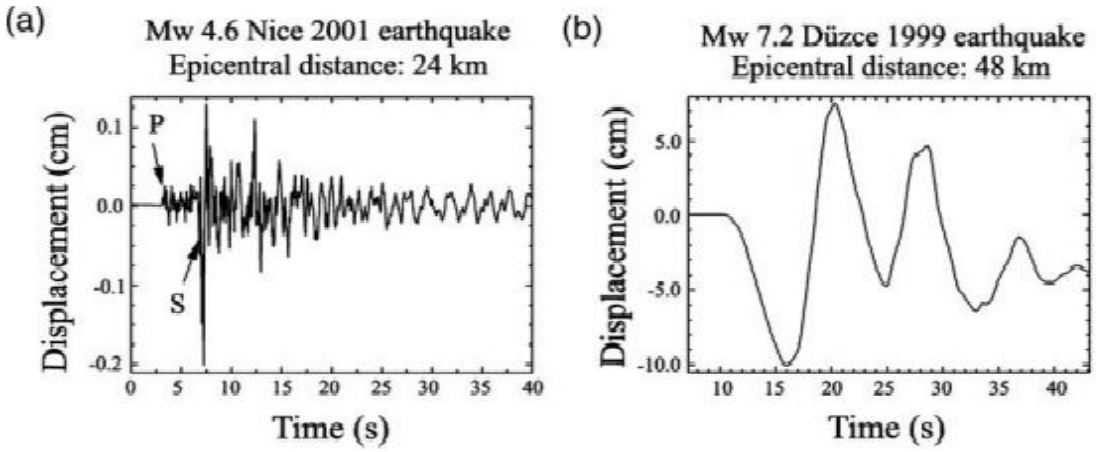

Figure 1.2. Waveform characteristics of near-source records for a moderate and a large earthquake. (a) Displacement seismogram at a distance much larger than the rupture dimension and individualized far-field P and S waves can be identified. (b) Displacement seismogram at a distance of the same order of rupture dimension P and S waves can not be distinguished (Delouis *et al.*, 2009).

2. SEISMOTECTONICS OF VAN REGION

2.1. General Remarks on the Active Tectonics of Turkey

Turkey is a tectonically very active country and has a long history of destructive earthquakes. It is a continuously deforming region surrounded by African, Arabian, and Eurasian major plates and located on the Anatolian and Aegean minor plates. Tectonics of this region is dominated by the collision of the Arabian and African Plates with Eurasia (McKenzie, 1972; Jackson and McKenzie, 1988) Figure 2.1.

Active tectonics of Turkey is the manifestation of collisional intracontinental convergence and tectonic escape-related deformation since the Early Pliocene about 5 Ma (Bozkurt, 2001). West of the October 23, 2011 event, earthquake tectonics are dominated by strike-slip faulting on East Anatolian Fault (EAF) in southern Turkey and North Anatolian Fault (NAF) in northern Turkey. These large, translational fault systems extend across much of central and western Turkey and accommodate the western motion of the Anatolian-Aegean block as it is being squeezed by the converging Arabian and Eurasian Plates (McKenzie, 1972) Figure 2.1.

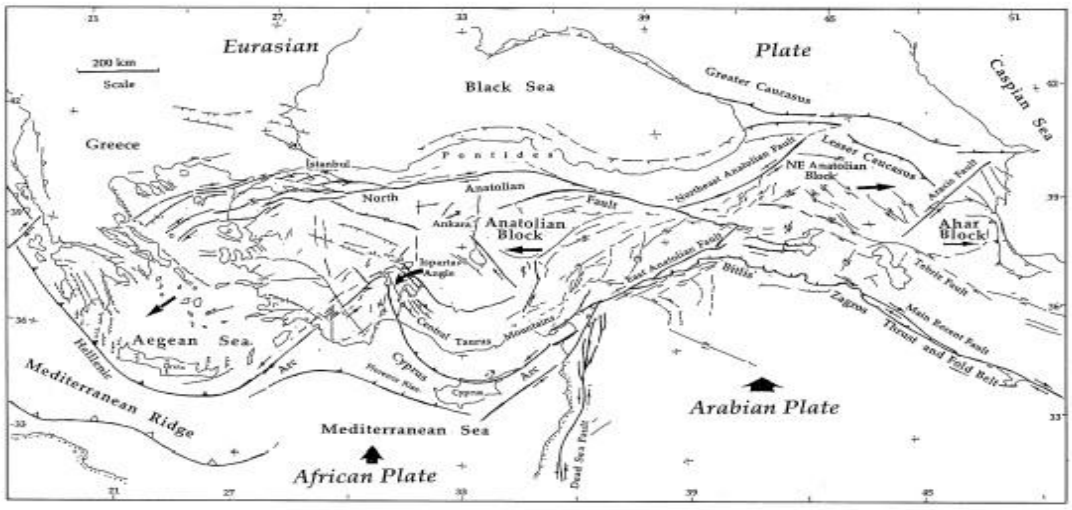

Figure 2.1. Relative motion of plates and distribution of active faults (Barka and Reilinger, 1997).

As it is cited in many papers such as (Barka and Reilinger, 1997), the plate tectonic model NUVEL-1A; (DeMets *et al*., 1990,1994) suggest that the Arabian Plate is moving in a north-northwest direction relative to Eurasia at a rate of about 18-25 mm/yr averaged over about 3 Ma. The northward motion of Arabia results in continental collision in the region of Lake Van along the Bitlis-Zagros fold and thrust belt (McKenzie 1972). As a consequence, an intense earthquake activity is observed. The smaller plates move away from the Lake Van region and the motion is transmitted to east and west as can be seen in Figure 2.1.

Geodetic analysis on GPS results provide direct estimates of Arabia-Africa-Eurasia motion, the counterclockwise rotation and associated westward motion of the Anatolian Plate, and the comparatively rapid southward motion of the southern Aegean region relative to Eurasia as shown in Figure 2.2. The apparently coherent motion of Anatolia (little internal deformation) is consistent with relatively strong continental lithosphere (Reilinger *et al*., 1997; Barka and Reilinger, 1997; Lundgren *et al*., 1998; McClusky *et al*., 2000).

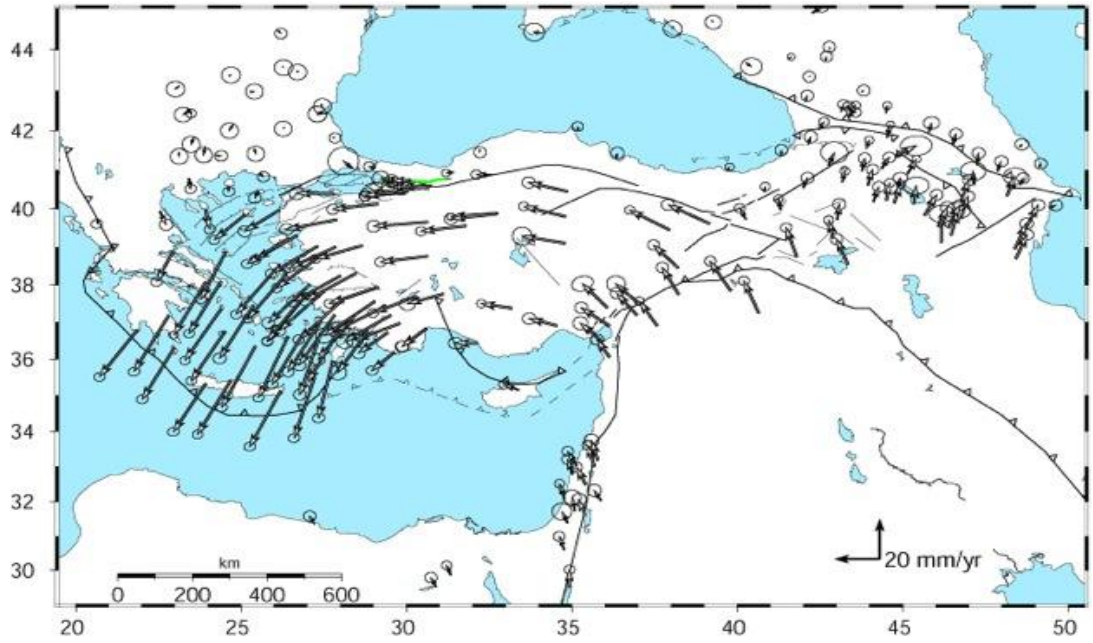

Figure 2.2. GPS-derived velocities (mm/yr) with respect to Eurasia.An illustration of the rotating velocity vectors and progressive increase in rate from the north Arabian platform to the Hellenic Trench.(Reilinger *et al.,* 2006).

The counterclockwise rotation of velocity vectors in Figure 2.2 characterized by east-west normal faults along Aegean, right lateral strike-slip motion along NAF, and right and left lateral and thrust faulting in the Eastern Anatolia,is explained primarily by the collision of the African Plate at the east (Reilinger *et al*., 2006).

2.2. Tectonic Characteristics of the Region Around Lake Van

The area of Lake Van and its surroundings belongs to the East Anatolian tectonic region of Turkey. The 23 October 2011 Earthquake tookplace near the center of the elevated Anatolian plateau to the east of the intersection point of North and East Anatolian Faults (Karlıova Junction). It is well known that the tectonics of this region is dominated by the Bitlis Suture Zone and Zagros fold and thrust belt.

The tectonics of the epicentral region were firstly studied in detail by (Tchalenko, 1977) some of the possible fault traces were indicated. Tchalenko argued that main faults of the region died out as they approach Lake Van. For instance it was assumed that NAF lost character because no major aftershocks had been observed to the east of Karlıova after 1939 Erzincan Earthquake. Furtherresearches on the active tectonics of the region indicate a complex source structure.

According to (Şaroğlu and Güner, 1981; Barka and Kadinsky-Cade, 1988) neotectonics in Eastern Anatolia involves four types of structures: NE-SW trending sinistral faults (Horasan-Narman Fault, Erzurum Fault Zone, Malazgirt Faults), NW-SE trending dextral faults (Çaldıran-Tutak-Karayazı Fault, Balıkgölü Fault), E-W trending thrusts (Muş- Van thrust) and N-S trending extension cracks and/or normal faults (giving rise to volcanic activity, Nemrut and Süphan Volcanoes), as explained in (Barka and Reilinger, 1997).

It is clear from Figure 2.3 that strike slip faulting is the most common faulting type in eastern Turkey. Compressive features, such as thrust faulting, which were obviously the primary faulting during the earliest stages of continental collision, are still active but are of lesser importance (Örgülü *et al*., 2003).

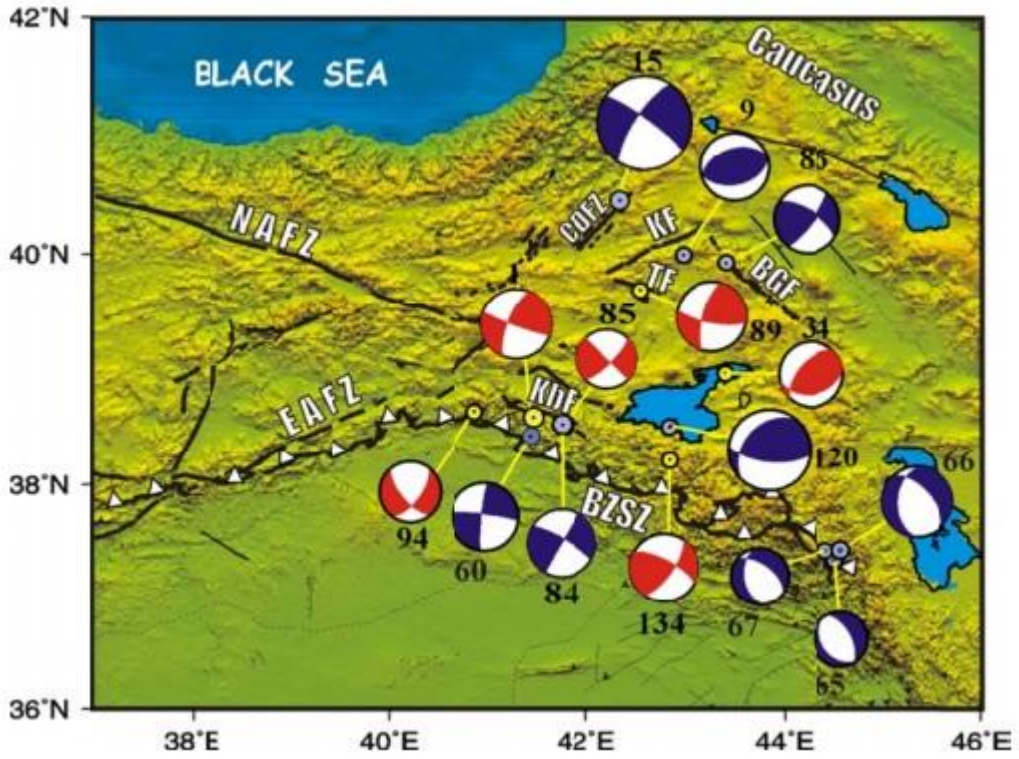

Figure 2.3. Focal mechanisms of selected eventsdistributed in Eastern Anatolian Plateau. Çobandere Fault zone (ÇDFZ), Kağızman Fault (KF), Tutak Fault (TF), Balık Lake Fault (BGF), Kavakbaşı Fault (KbF) (Örgülü *et al*., 2003).

Although a large number of detailed investigations have been realized on the active faults in East Anatolian tectonic region, according to the current report by Kandilli Observatory and Earthquake Research Institute, the only active or probably active tectonic element in the epicentral region of 23 October, 2011 Van Earthquake is mapped by (Koçyiğit *et al*., 2002) as shown in Figure 2.5. On the other hand, the pure reverse character of the recent Van Earthquake is not in accordance with the strike-slip character of the fault mapped by (Koçyiğit *et al*., 2002). There are several attempts to remove the ambiguity on the source of the October 23, 2011 Earthquake. For instance, it is claimed in (Taşkın, 2013) that the October 23, 2011 Earthquake took place on "Van Fault", which is recently discovered and is not available in the Active Fault Map of Turkey (Emre *et al.*, 2011).

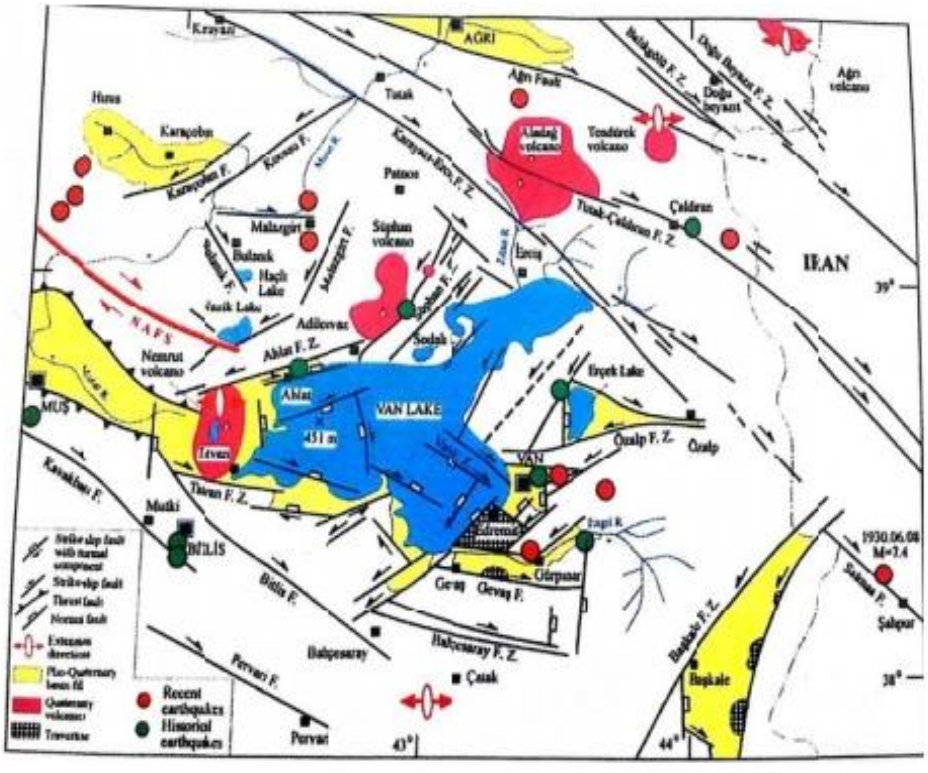

Figure 2.4. Active faults in the vicinity of Lake Van prepared by (Koçyiğit *et al*., 2002).

2.3. Seismicity of the Region

In this section we give a historical seismic backround of Van region that had been already studied by researchers. The 23 October 2011 Earthquake caused heavy damage in Van and several towns and villages around Lake Van. It was followed by several aftershocks and another strong event (Mw5.7) that occurred on 9 November 2011, causing further damage and casualities.The historical seismicity of the area is described by some regional parametric earthquake catalogs (Soysal *et al*., 1981; Shebalin and Tatevossian, 1997; KOERI-NEMC for the instrumental period) and has been the subject of several studies, such as Tchalenko (1977), Ambraseys (1989, 2001), and Ambraseys and Jackson (1998) as cited by a recent study (Albini *et al*., 2012) which is in search of an event with equivalent size to the 23 October 2011 Earthquake. According to this study no earthquake with a magnitude equivalent to the 2011 one is reported by the catalog in the area of the 2011 Earthquake; so, apparently, there are no predecessors of this earthquake. Also It is stated that there are no earthquakes which could, in principle, be underestimated or mislocated by the catalog and that could be relocated in the area of the October 2011 Earthquake with a comparable magnitude Figure 2.5.

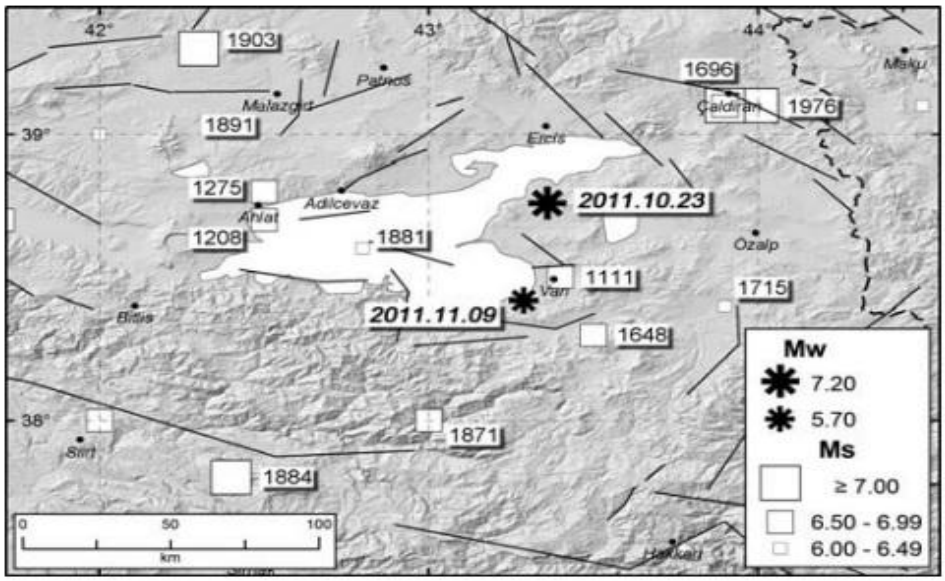

Figure 2.5. Earthquakes in the investigated area from Shebalin and Tatevossian (1997). The black asterisks show the epicenters of the 23 October and 9 November 2011 Earthquakes. Documented from (Albini *et al*., 2012).

The highly complex and heterogeneous characteristics of the compressional regime in the region has been testified by previous earthquake activities such as M_L 6.9 1966 Varto Earthquake with thrust faulting while M_L7.6 1976 Çaldıran Earthquake was caused by a strike-slip faulting. Historical records indicate that several destructive earthquakes shake the region as listed in Table 2.1 which is documented from (Taşkın *et al*., 2013). Note that the earthquake events prior to the twentieth century are described by their intensities and for those occured in instrumental period M_S (surface magnitude) values are used.

Table 2.1. Historical earthquakes of Van and the surroundings.

Date	Location	(I) or (M_S)
Historical earthquakes in terms of intensity (I)		
?.?.1012	Malazgirt, Mus	VII
?.?.1110	Central Van	VIII
?.?.1245	Van-Ahlat-Bitlis	VII
?.?.1363	Mus	VIII
?.?.1441	Van-Bitlis-Mus	X
02.04.1647	Van-Bitlis-Mus	IX
?.?.1685	Central Van	VI
?.?.1701	Central Van	VIII
?.?.1704	Central Van	VII
?.?.1715	Ercis, Van	VIII
30.05.1881	Van-Bitlis-Mus	IX
?.?.1892	Malazgirt, Mus	VI
Instrumental period events in terms of magnitude (M_S)		
29.04.1903	Malazgirt, Mus	6.7
10.09.1941	Ercis, Van	5.9
20.11.1945	Catak, Van	5.8
19.08.1966	Varto, Muş	6.9
16.07.1972	Central Van	5.2
24.11.1976	Caldiran, Van	7.5
26.03.1977	Ercis, Van	5.2

3. DATA AND METHOD

3.1. Historical Remarks on Strong-Motion Seismographs

The first clear record by strong-motion seismograph was obtained in 1940 Imperial Valley Earthquake (El Centro Earthquake) which has magnitude 7.1 and peak ground acceleration 300 gal. Until this event, recording large earthquakes had not been possible because thepencil of the recording seismograph was leaping up before buildings and other things. The problem was resolved with the invention of strong-motion seismographs. A strong-motion seismogram has been designed in such a way that it can record a faithful representation of the acceleration waveform without being damaged under destructive earthquakes. At this point strong-motion seismograph is similar to the flightrecorder, which protect all the information about the flight even if there is plane crash. Thus strong-motion seismographs are very useful instruments for getting information about earthquakes in the near-field region where the destructive effect of earthquake is generally higher (Yorihiko, 1976).

3.2. Strong-Motion Network Near the Earthquake

In this study, the strong-motion network of Prime Ministry Disaster and Emergency Management Presidency has been used. The Mw7.2 Earthquake was recorded by 22 stations within the region, most of them at large distances beyond 100 km (Figure 3.1). However the closest Muradiye station (46 km) strong motion recording which is located in Van city center, lost its energy during the event. The stations list and related PGA values can be seen below (Table 3.1).

Figure 3.1. The map showing the epicenter location and 22 strong-motion stations (web site of AFAD. http://kyh.deprem.gov.tr/ftpe.htm).

Table 3.1. The closest stations and corresponding PGA values.

Station	hypocentral distance	PGA
Van Muradiye (No. 6503)	46 km	178.5 cm/s^2
Muş Malazgirt (No. 4902)	97 km	56.0 cm/s^2
Bitlis Merkez (No. 1302)	117 km	102.2 cm/s^2
Agri Merkez (No. 0401)	122 km	18.5 cm/s^2

Furthermore we could not use records of the station at Muş Malazgirt because it had an old type of accelerometer and had lost the initial part of P-wave which we need to use. The relatively high PGA (peak ground acceleration) value at Bitlis, where much damage has been reported may be caused by the EW extension of the ruptured fault (http://earthquake-report.com/2011/10/24/understanding-the-7-2-magnitude-earthquake-in-east-turkey-october-23-2011/). Also site effect may be responsible for this situation. Since all other stations are at larger distances and most of them could not record the initial part of P-wave than we used only Bitlis and Ağrı stations in our calculations. Strong-ground motion recording properties and header values can be seen in Appendix A. It is also possible to reach real acceleration values (uncorrected raw data) from the web page of AFAD given at the end of references.

3.3. The Use of Strong-Motion Records for Magnitude Determinations

It is well known that the widely used magnitude scales, M_L (local magnitude) and M_S (surface wave magnitude) and m_b (body wave magnitude) suffer saturation when the rupture dimension of the earthquake exceeds the wavelength of the seismic waves (usually 5-50 km) used for magnitude determination (Kanamori, 1977). By considering the reported M_L values it is seen that the upper limit to M_L is near 7.

In the range of $3< M_L< 7$, the M_0- M_L relationship empirically defined by (Thatcher and Hanks, 1973) is almost the same with the M_0-M_W relationship defined in (Kanamori,1977; Hanks and Kanamori, 1979):

$$M_W = (2/3)\log(M_0) - 10.7 \qquad (3.1)$$

Thus a remarkable coincidence between $M_L$and M_W is expected in this range (Table 3.2).

Table 3.2. Seismic Moments and Magnitudes for Southern California Earthquakes (1918-1973) documented from **(**Kanamori and Hanks, 1979).

Date	M_0, $\times 10^{25}$ dyn cm	M_L	M_s	M
April 21, 1918	15		6.8	6.8
July 23, 1923	1		6¼	6.0
June 29, 1925	20		6¼	6.8
Nov. 4, 1927	100, 65*		7.3	7.3, 7.2
March 11, 1933	2	6.3	6¼	6.2
May 19, 1940	30	6.4†	6.7	7.0
July 1, 1941	0.9	5.9	5.9	6.0
Oct. 21, 1942	9	6.5	6½	6.6
March 15, 1946	1	6.3	6¼	6.0
April 10, 1947	7	6.2	6.4	6.5
Dec. 4, 1948	1	6.5	6.5±	6.0
July 21, 1952 (main shock)	200	7.2‡	7.7	7.5
July 21, 1952 (aftershock)	3	6.4		6.3
July 29, 1952 (aftershock)	3	6.1		6.3
March 19, 1954	4	6.2		6.4
April 9, 1968	6	6.4	6.7	6.5
Feb. 9, 1971	10	6.4	6.6	6.6
Feb. 21, 1973	0.1	5.9	5.2	5.3

Unless otherwise specified, M_0 entries are from *Hanks et al.* [1975], and M_L entries from *Hileman et al.* [1973]. All but the last three M_s entries are from *Gutenberg and Richter* [1954], taken as M_s according to *Geller and Kanamori* [1977]. M_s for April 9, 1968, and February 9, 1971, are from *Kanamori and Anderson* [1975], and M_s for February 21, 1973, is from the National Earthquake Information Service, U.S. Geological Survey.

*From *Yeh* [1975].

†From *Trifunac and Brune* [1970].

‡From *Bolt* [1978].

As it can be seen, in case of the Imperial Valley (1940) Earthquake, M_L is 0.6 units less than M_W, revealing anomalously low 1-s ground motion amplitudes for what is otherwise a fairly large earthquake by California standarts. In case of Kern County (1952) main shock, $M_L$is 0.5 units less than M_S and 0.3 units less than M_W, almost reflecting the saturation level of M_L around 7. Deviations of M_W from M_S or M_L can in most cases be attributed to variable stres drop or saturation of M_L and M_S (Hanks and Kanamori, 1979).

For the recovery of the M_L value, an attempt was done by Kanamori and Jennings (1978). In fact, they presenteda technique for determination of local magnitude $M_L$using strong-motion accelerograms probable for the first time. The accelerograph records are used as an acceleration input for the equation of motion of the Wood-Anderson torsion seismograph to produce a synthetic seismogram which is then read in the standard manner. It is possible to obtain senthetic displacement seismograms in places where real recordsare not reliable. Although they could obtain slightly larger M_L values

the results differed significantly from M_W values. An average value of M_L = 7.2 is obtained for the 1952 Kern County Earthquake which is still less than M_W value (Table 3.2).

A typical example of this situation is confronted in case of the October 23, 2011 Van Earthquake (M_L 6.6 vs M_W 7.2). Here M_W is the moment magnitude obtained from the far-field displacement spectrum of body waves. In such cases local magnitude determinations are deceptive. Hence, there is a need to find a way for the determination of M_W from near-field records too.

Recent studies such as Allen and Kanamori, (2003), Wu and Teng (2004); Wu and Kanamori, (2008) using strong-motion records brought about new methods to calculate moment magnitude from near-field records. One of these is the MWSYNTH method developed by Delouis *et al.* (2009) which provide suitable results for near real-time fast determination of moment magnitude.

3.4. The MWSYNTH Method

The aim of the method is to determine moment magnitude of earthquakes immediately after occurrence, before any source or focal mechanism inversions have been performed. The only prerequisites are the hypocenter location and the detection of first P-wave arrival at each station.

Before any earthquake is analyzed, synthetic seismograms are generated for a series of hypothetical finite dimension sources. The synthetic seismograms include effects of source finiteness as well as the complete displacement field (near, intermediate, and far field) generated in a simple 1D layered velocity model.

Using synthetic displacement spectra, it is shown that the spectral level, the spectral plateau at low frequency, scales with moment magnitude (Delouis *et al*., 2009). More specifically, the spectral level is the maximum value of the displacement spectra at low frequency, corresponding to the spectral plateau.

To determine the moment magnitude of a specific earthquake the displacement spectra of the observed records are computed, and the corresponding spectral levels are compared to those obtained from synthetic spectra computed for a variety of finite dimension source models. Each source model is sized according to a specific seismic moment, hence to moment magnitude.

To assess the possibility of obtaining early estimates of the moment magnitude, and to analyze how the length of the time window influences the value of the computed magnitude, spectra are calculated for different time windows.

3.4.1. Synthetic Seismograms and Tables of Spectral Levels

Focal mechanism influences the displacement spectrum via the radiation pattern. To obtain reliable results the effects of various focal mechanisms are averaged. Synthetic seismograms are generated for six different focal mechanisms; which are specified by (strike/dip/rake= 0/90/0, 90/90/0, 0/45/90, 90/45/90, 45/45/90, and 135/45/90) respectively.

They correspond to strike-slip and dip-slip faulting. For a station located 1–100 km from the epicenter in the single azimuth N70°E arbitrarily chosen see (Figure 3.2).

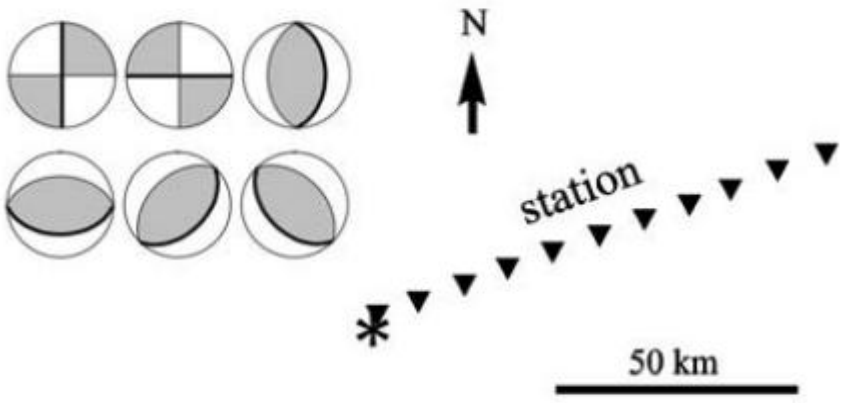

Figure 3.2. The six different focal mechanisms (rupture plane in bold) and relative position of the seismic stations (black triangles) with respect to the hypocenter (star) used to compute the synthetic seismograms (Delouis *et al*., 2009).

For Bitlis station we produced synthetics at 110 km, 115 km, 117 km, and 120 km distances in the azimuth N258°E. And for Ağrı station we produced synthetics at 115 km, 120 km, 122 km, 125 km in the azimuth N341°E. For calculations of distances and azimuths see Matlab commands used in Appendix B.

The values stored in Table D.2 in Appendix D are the spectral levels averaged over the three components (north–south, east–west, and vertical) of the seismograms and over the six different focal mechanisms. A table of synthetic spectral levels is shown in Figure 3.4.

The method is initially developed for earthquakes occurring only at shallow depth (<50 km) and with epicentral distances less than 100 km. However, the approach could be extended for deeper events and larger distances (Delouis *et al*., 2009). In this study we test the method for the 23 October 2011 Van Earthquake (depth=19 km) at epicentral distances about 120 km.

The hypothetical rupture plane is square for small to moderate earthquakes whose rupture does not reach the surface, and rectangular, more stretched along strike than along dip, for larger ones (Figure 3.3).

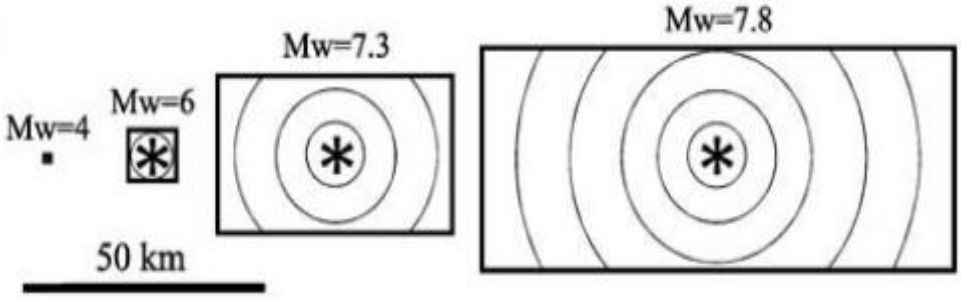

Figure 3.3. Dimensioning of the kinematic source models used to generate the synthetic seismograms as a function of moment magnitude (Delouis *et al*., 2009).

Rupture area is derived from the regression relations of Wells and Coppersmith (1994). The dislocation (slip), assumed constant on the fault, is determined from the relation $\Delta u = M_0/\mu lw$ where μ is rigidity and l, w are rupture length and width, respectively. M_0 is obtained from M_W using the Equation of Kanamori (1977) (Delouis *et al*., 2009).

The complete displacement field generated by the source is computed in the original method by using the discrete wavenumber method of Bouchon (1981). Instead of Bouchon (1981) we have used FK-method by (Zhu L., 2011) for a 1D layered velocity model (prepared by Hayrullah Karabulut using aftershocks of 2011 Van Earthquake) as shown in Table 3.3.

Table 3.3. Velocity Model.

Layer	thick	Vp	Vs	rho	Qa	Qb
1	2.00	3.80	2.00	2.30	0.40E+03	0.20E+03
2	2.00	4.00	2.15	2.35	0.40E+03	0.20E+03
3	3.00	4.50	2.35	2.45	0.40E+03	0.20E+03
4	3.00	4.50	2.35	2.45	0.40E+03	0.20E+03
5	8.73	6.10	3.50	2.75	0.80E+03	0.40E+03
6	9.27	6.10	3.50	2.75	0.80E+03	0.40E+03
7	16.00	6.30	3.60	2.80	0.80E+03	0.40E+03
8	8.50	7.20	4.00	3.10	0.80E+03	0.40E+03
9	50.00	8.20	4.70	3.40	0.12E+04	0.50E+03
10	50.00	8.20	4.70	3.40	0.12E+04	0.50E+03

source depth = 18.7 km at top of layer 6

The FK method calculates a trapezoidal source time function according to the size of the rupture, in other words for each magnitude value it calculate the corresponding source time function. Firstly Green's functions are generated at distances of concern then the corresponding waveforms (velocity or displacement) are formed.

Example 3.1. Generation of Green's functions and synthetic waveforms with FK method. ./fk.pl -MEAn/18.7 -N1024/0.1/2/0.1/0.1 110 115 117 120 125

This command generates Green's functions at 110, 115, 117, 120, and 125 km according to the velocity model MEAn, which is shown in Table 3.3 and 18.7 is the centroid depth of earthquake. Then if we want to obtain synthetic displacements at 117 km and in the azimuth N258°E (Bitlis station) we have the following command; ./syn –A258 -Md7.15/250/45/60 -OBITLIS -I -GEAn_18.7/117.grn.0

In this example synthetics are formed according to magnitude 7.15 and focal mechanism strike/dip/rake=250/45/60. General explanations of these commands can be seen in Section 5 of Appendix B.

The spectra of synthetic displacement seismograms are computed for different time windows and highpass frequencies. We define seven signal windows, ending 30, 40, 50, 60, 70, 80, 90 sec after earthquake origin time (a proper time window should include first P-wave arrival plus 3 seconds).In the dataset no station was close enough to the hypocenter to provide a magnitude estimate with time windows shorter than 30 s. Highpass frequencies are determined for Bitlis and Ağrı stations according to procedure explained in Section 3.4.2 (Figure 3.4).

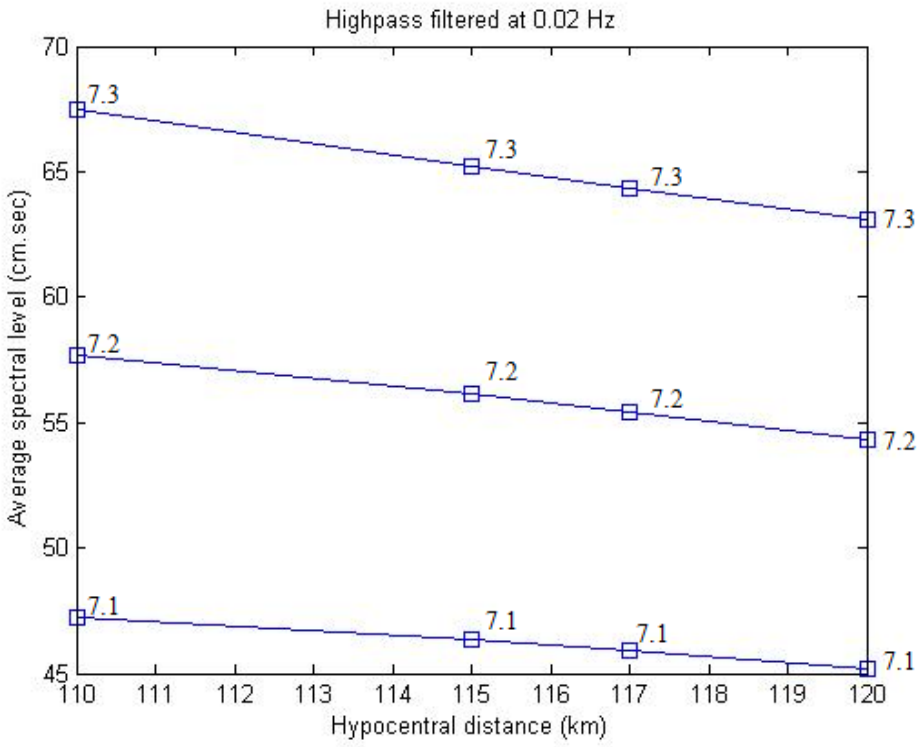

Figure 3.4. Average spectral level as a function of hypocentral distance and moment magnitude for synthetic displacement seismograms high-pass filtered at 0.02 Hz. Synthetic spectral levels are computed at certain distances (including epicentral distances).

The spectral level (highest value on the displacement spectra) is averaged over the three components of the seismograms and over the six different focal mechanisms shown in Figure 3.2. Labels on the curves indicate moment magnitude (7.1 - 7.3). Computed for a time window ending 80 sec after origin time.

Precomputing of synthetic seismograms and construction of tables of spectral levels are performed only once. The processing of real records and determination of Mw by interpolation in the tables of synthetic values could be implemented as a real-time automated procedure.

3.4.2. Processing of Strong-Motion Records

Initial processing of real seismograms includes computing the average amplitude of the preevent noise (3 sec preceding the first Parrival), subtracting it from the wholesignal, and cutting the record at the end of the selected time window. It may happen that reverberating waves generated in the shallow crustal layers dominate in the late section of the displacement records, beyond the direct contribution of the source. Those late arrivals can affect the displacement spectrum at low frequency, resulting in an overestimation of the magnitude. To limit this effect we perform a test on the acceleration level in a similar way as in Wu and Teng (2004). If acceleration decreases to less than 20% of the overall maximum acceleration and remains below that threshold during five contiguous seconds, the source contribution is assumed to be completed and the following part of the signal is set to amplitude zero (Delouis *et al*., 2009). The Matlab codes that we prepared for these processings can be seen in Appendix B.

The frequency response of digital accelerographs is nominally flat in acceleration from direct current (DC), or 0 frequency to 50 Hz, but baseline offsets are usually observed during seismic shaking. These offsets in acceleration can produce unreasonable displacements after double integration and contaminate the displacement spectra at low frequency. To overcome this problem spectral levels are computed after high-pass filtering. This is done by analyzing the shape of the acceleration spectrum at low frequency. Theoretical acceleration spectra in the far field are characterized by f^2 rise at frequencies below the corner frequency, followed by a plateau (Aki and Richards, 1980). Near-field synthetic seismograms reveal a steady rise at low frequency, although not necessarily as f^2. In the absence of noise the acceleration spectra exhibit a continuous rise in the initial part followed by a plateau or decay in the midhigh frequency range. This characteristic behavior is observed for real acceleration records unaffected by baseline shifts. On the other hand, baseline shifts induce an over amplification of the lowest frequencies, resulting

in a strong curvature of the low-frequency part of the acceleration spectrum, which becomes V-shaped (Figure 3.5b). The point of maximum curvature at low frequency, corresponding to the bottom of the V-shape where the variation of the slope is at its maximum, can be used to define an effective high-pass cutoff frequency to remove the low-frequency noise (Delouis *et al*., 2009).

(a)

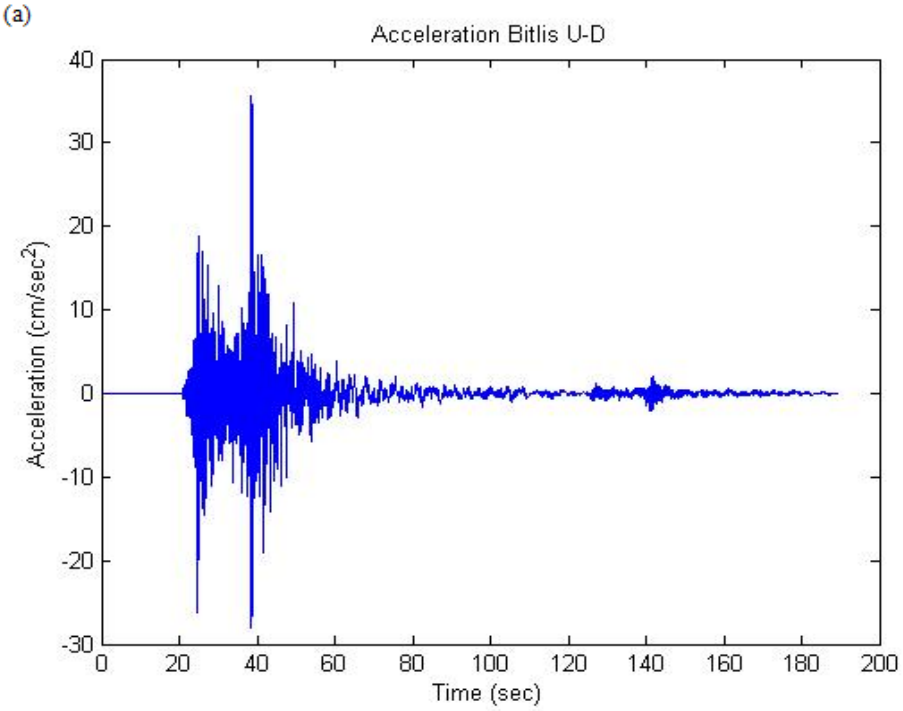

(b)

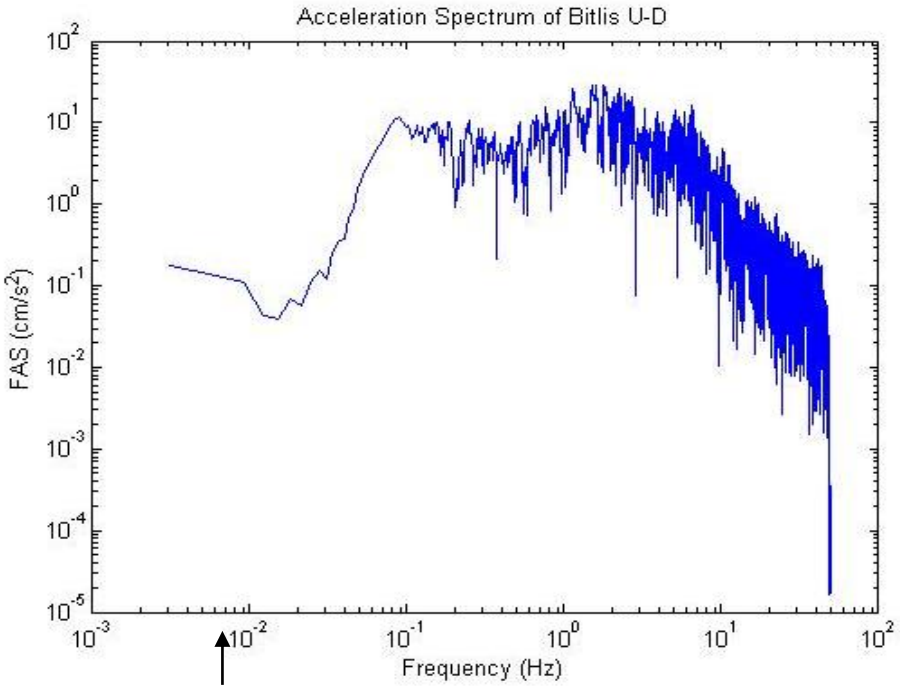

Figure 3.5. (a) Vertical component of the Acceleration for Bitlis station after initial processing (b) Acceleration spectrum corresponding to part (a), the high-pass frequency for U-D component is approximately 0.015 Hz.

Notice the initial decay in the spectrum of acceleration which implies baseline shifts. By just looking at the acceleration spectrum we have approximately choosen the high-pass cutoff frequency. For a given station we apply a single high-pass frequency, selected as the highest value among the high-pass frequencies found for the three components. The spectrum of all components and the corresponding approximate high-pass cutoff frequency values are available in Appendix C. We use 0.02 Hz for Bitlis and 0.04 Hz for Ağrı stations.

According to Delouis *et al*. (2009) a minimum requisite for a given window to be used is that it should include the first P-wave onset and the next three seconds. Since we use data from stations at hypocentral distances about 120 km, P-wave arrivalsare greater than 20s (20.33s for Bitlis and 22.78s for Ağrı). That's why we choose windows longer than 20s. For an automated selection of the optimal high-pass filtering frequency from the curvature of the initial part of the spectrum, the window should include the S-wave onset and the next 20 sec of signal (Delouis *et al*., 2009). In case of a time window shorter than the arrival time of Swave plus 20 sec, the high-pass frequency is fixed in a conservative way to 0.25 Hz. This was included at the beginning of the development of the method in testing the method with short time windows for early warning. Time windows for which the signal may be too short for a spectral analysis are not normally used.

3.4.3. Computing of Mw

In order to get rid of the effects of baseline shifts, after having integrated twice the acceleration records, we apply the selected high-pass filters, and then compute the displacement spectra. We retrieve the spectral level as the maximum amplitude of the low frequency part of the displacement spectrum and compute the average spectral level over the three components of the seismograms. These average values can then be compared with those computed for the synthetic seismograms.

We compute the moment magnitude Mw for the differenttime windows defined in previous Section: 30, 40, 50, 60, 70, 80, and 90 sec after origin time. For each station we select the prestored table of synthetic data corresponding to the same time window and high-pass frequency used to process the observed seismograms. Each table contains the average synthetic spectral levels as a function of magnitude for different predetermined hypocentral distances (Figure 3.4). For each station the moment magnitude corresponding to the observed spectral level and to the actual hypocentral distance is found by interpolating in the table values. Example 3.1 illustrates the process with station Bitlis, which recorded the 23 October, 2011 Van Earthquake.

For each time window Mw is determined as the weighted average of the Mw computed for the individual stations. Considering that the spectral level is better defined and more representative of the actual seismic moment when the low frequencies are better preserved, weight is chosen as the inverse of the high-pass frequency. If more than three stations are available a standard deviation is computed (Delouis *et al*., 2009). When the low frequencies are too strongly filtered out a saturation of spectral levels occurs for large magnitudes. Accordingly, we had to define some thresholds for magnitude as a function of the high-pass frequency. Moment magnitude M_W is limited to values 7.0, 7.3, and 7.6 for high-pass frequencies larger than 0.3, 0.1, and 0.08, respectively (Delouis *et al*., 2009). We select the average magnitude computed with the 90 sec time window as the earthquake moment magnitude because the displacement becomes constant 90 sec after the origion time (Figure 3.6).

(a)

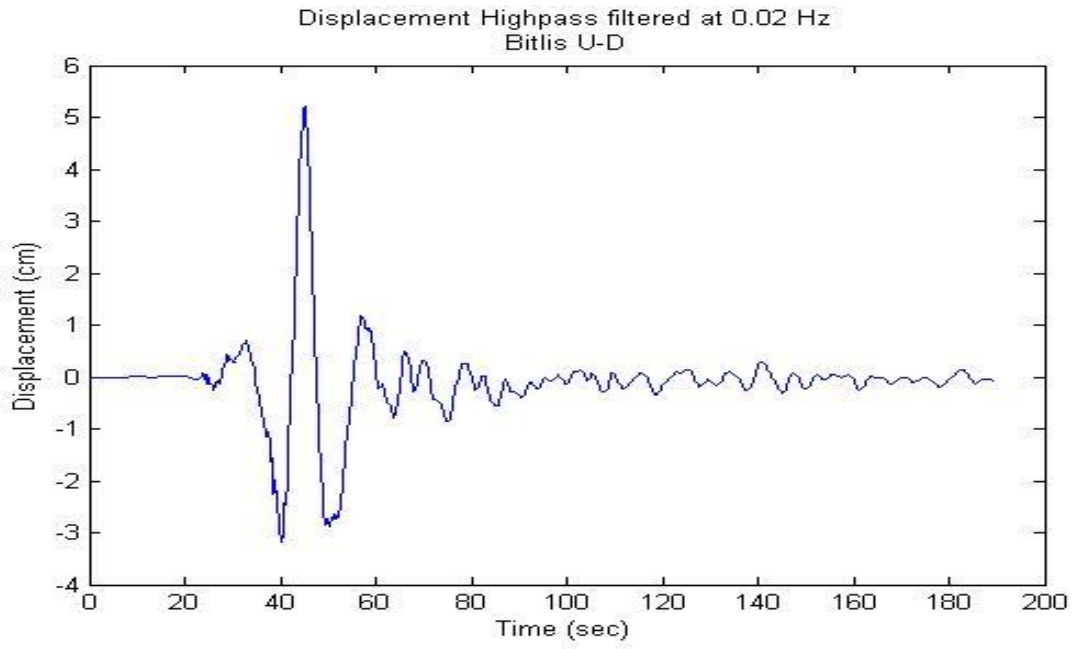

(b)

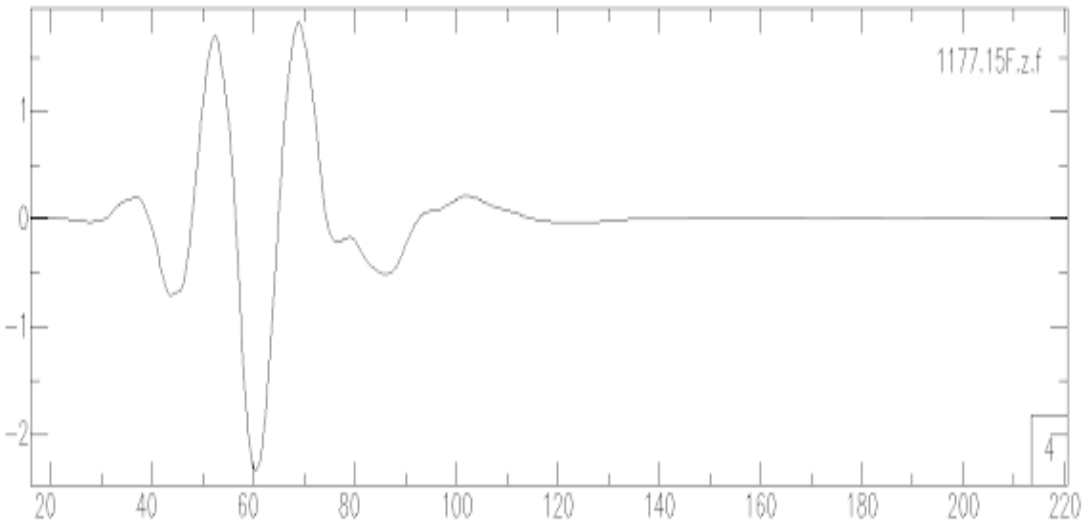

Figure 3.6. Comparison of the real and synthetic displacement seismograms. (a) Vertical component of the real displacement seismogram of station Bitlis high-pass filtered at 0.02 Hz. (b) Vertical component (high-pass filtered at 0.02 Hz) of the corresponding synthetic displacement seismogram at the epicentral distance and azimuth (117 km, N258°E) resulting for MW=7.15.

Example 3.2. Procedure for computing M_w.

(a)

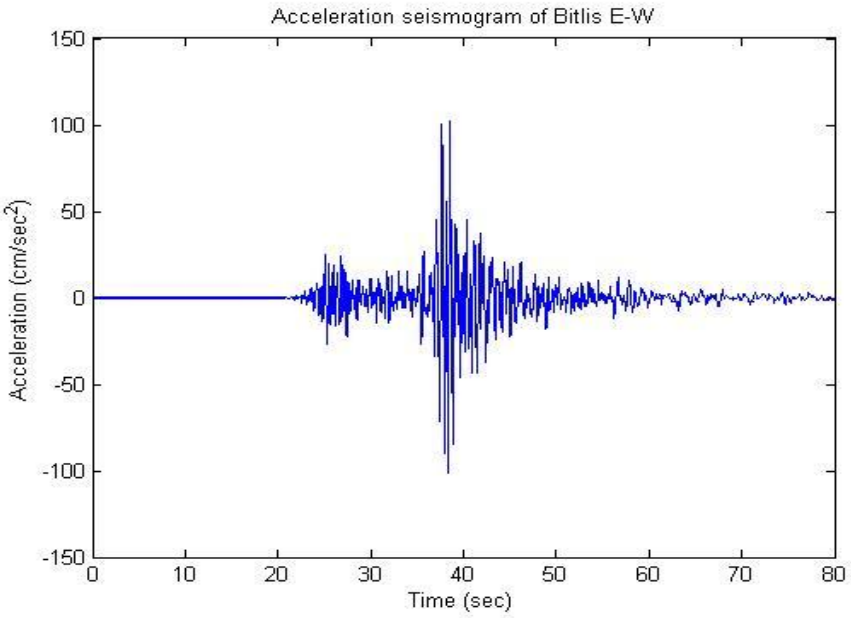

(b)

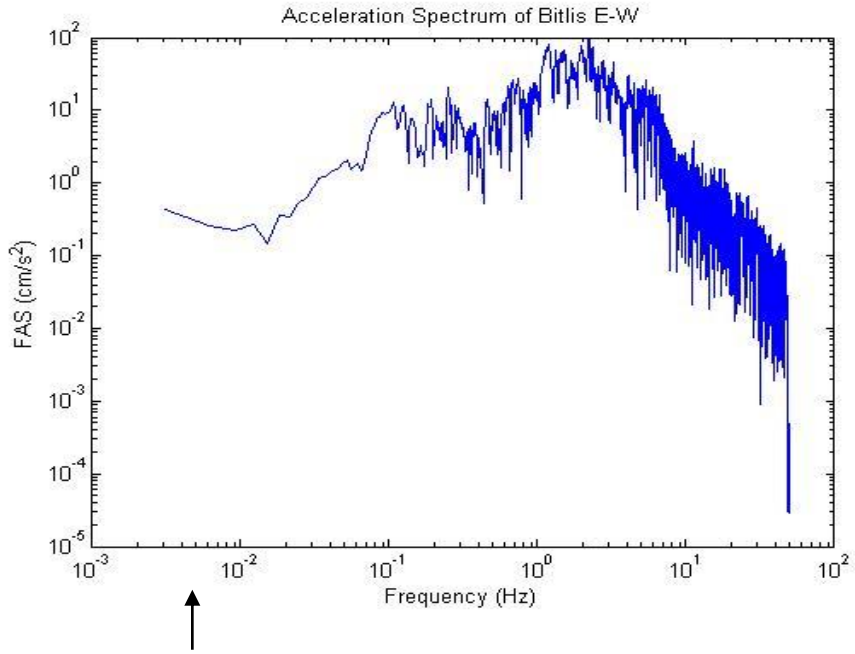

Figure 3.7. The point of maximum curvature at low frequency, corresponding to the bottom of the V-shape is about 0.015 Hz as shown with an arrow. (a) Acceleration time history for 80 sec window of Bitlis station (E-W component). (b)Determination of the high-pass frequency from the acceleration spectra.

However we use 0.02 Hz which is the highest value among three components. See Appendix C.

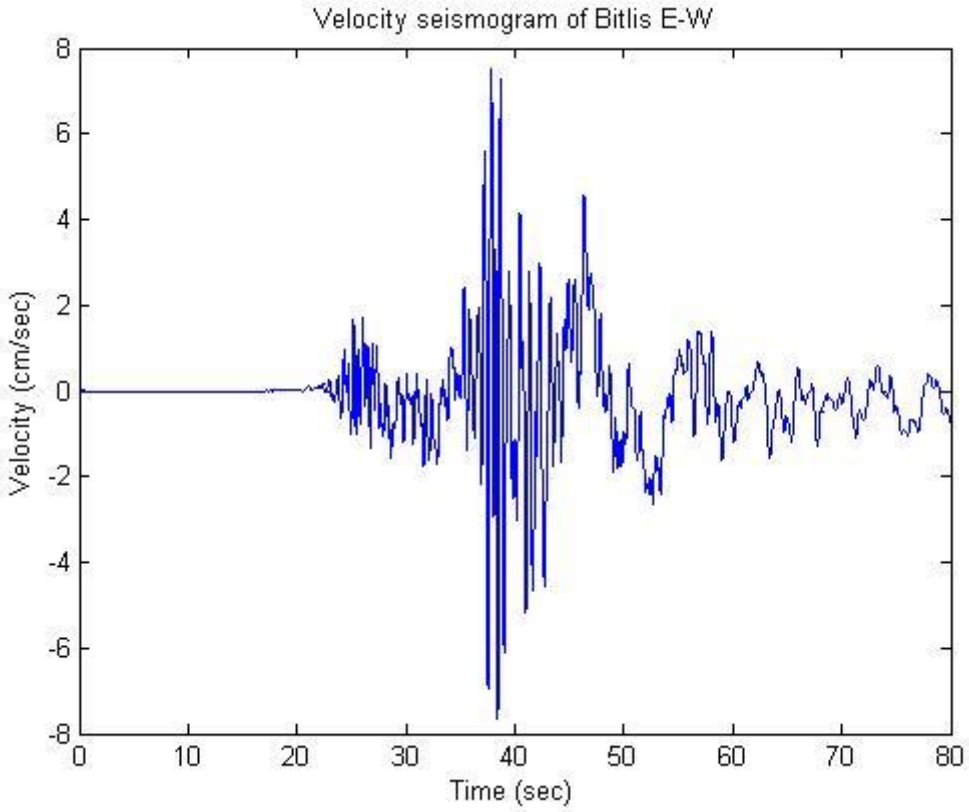

Figure 3.8. Velocity seismogram integrated from Figure 3.7 (a). As can be seen the slope of the different parts of the velocity seismogram is not the same. This means there are baseline shifts in acceleration seismogram.

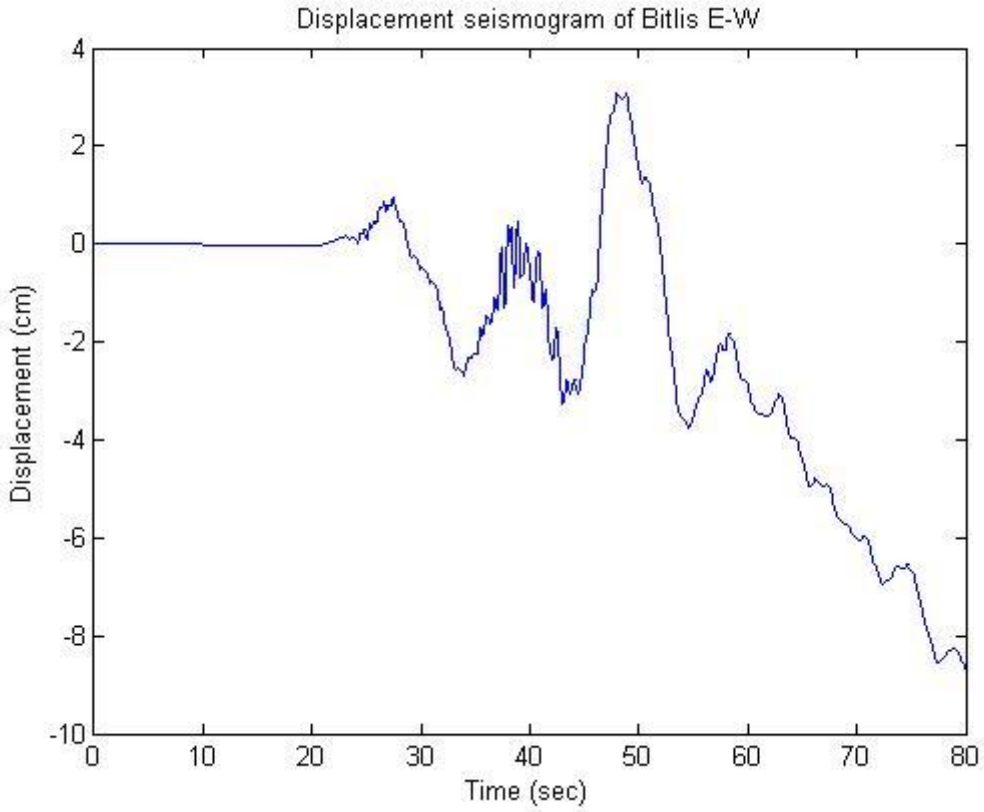

Figure 3.9. Displacement seismogram integrated from Figure 3.8. Resulting from the uncorrected baseline shift an unreasonable displacement above 8 cm is observed for Bitlis station located at 117 km from hypocenter.

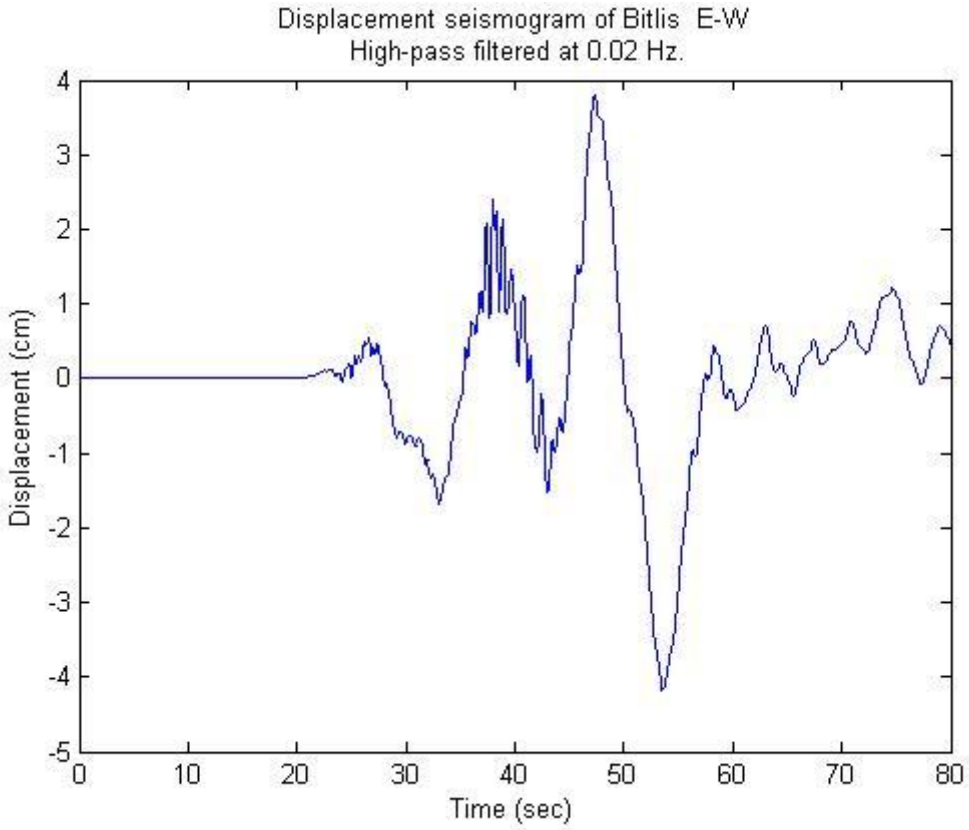

Figure 3.10. Displacement seismogram high-pass filtered at 0.02 Hz from Figure 3.9. Thus strong-motion record is integrated to displacement and high-pass filtered at 0.02 Hz to remove the baseline shift artifacts.

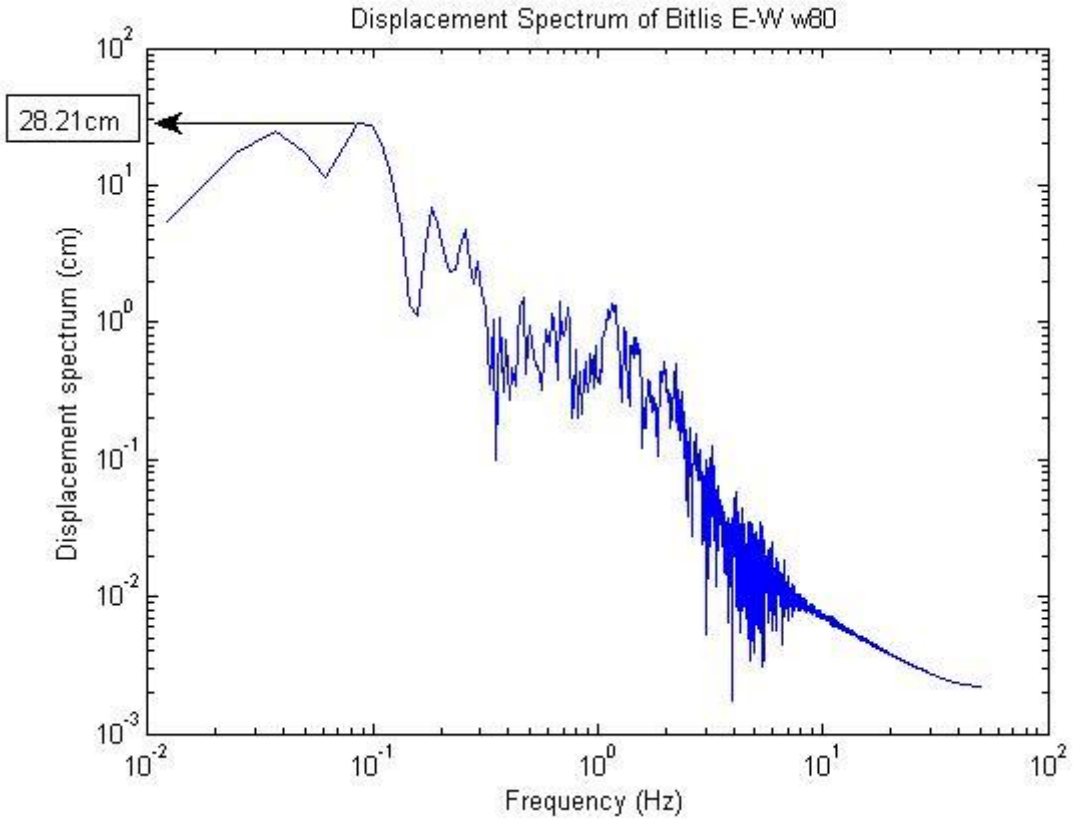

Figure 3.11. Displacement spectrum obtained from the fast Fourier transform of Figure 3.10. For 80 sec time window (w80) of the east component of station Bitlis, the spectral level is 28.21cm. The moment magnitude corresponding to the spectral leveland to the hypocentral distance (117 km) is obtained by interpolation within the table, as shown in part (g).

The code we prepared in MATLAB to obtain spectral levels can be seen in Section 4 of Appendix B. For the list of all displacement spectral levels (for each station, window and component) see Table D.1. in Appendix D.

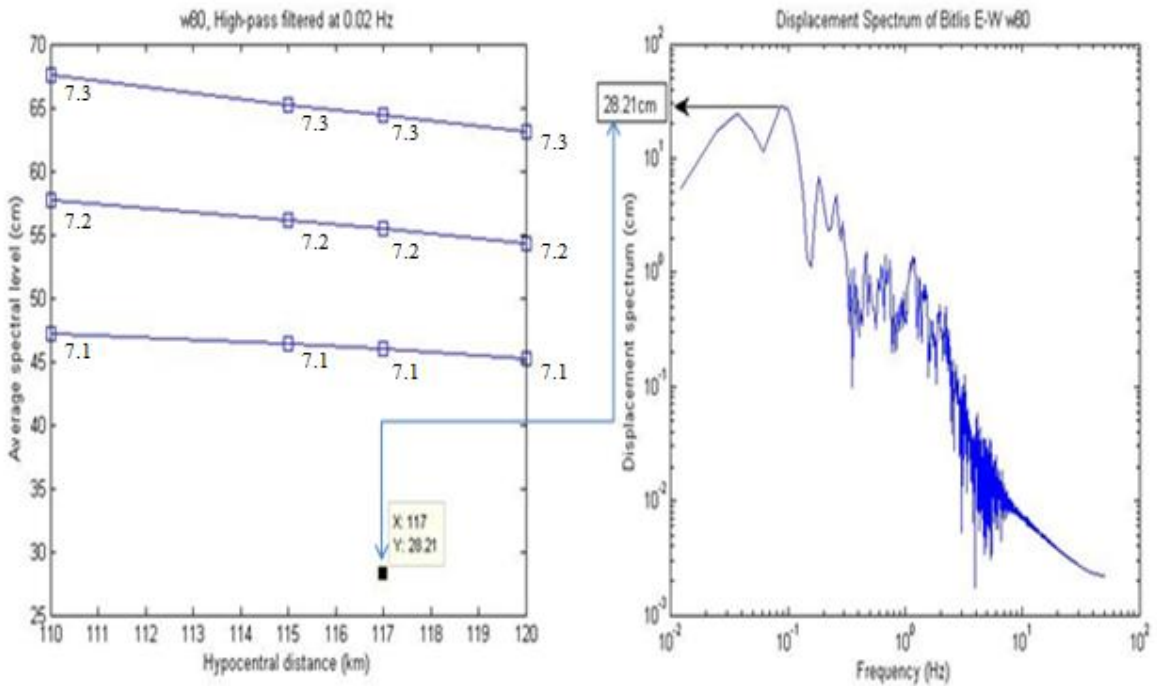

Figure 3.12. Scheme illustrating the principle of moment magnitude determination. On the left, graphical representation of a table of precomputed values of average spectral level as a function of magnitude and hypocentral distance, for synthetic displacement seismograms high-pass filtered at 0.02 Hz.

Labels on the curves indicate moment magnitude. On the right, Displacement spectrum obtained in part (f). The black point on the left is representing the moment magnitude calculated from this record. In this figure only the east component of station Bitlis is shown for the sake of simplicity, whereas in fact we average the values over the three components. With this component the magnitude is less than 7.1.

4. RESULTS

The representation of the real spectral levels in the tables of synthetic spectral levels are shown in the following graphs which are prepared from both synthetic and real spectral levels values. Numerical values of spectral levels are all listed in Appendix D.

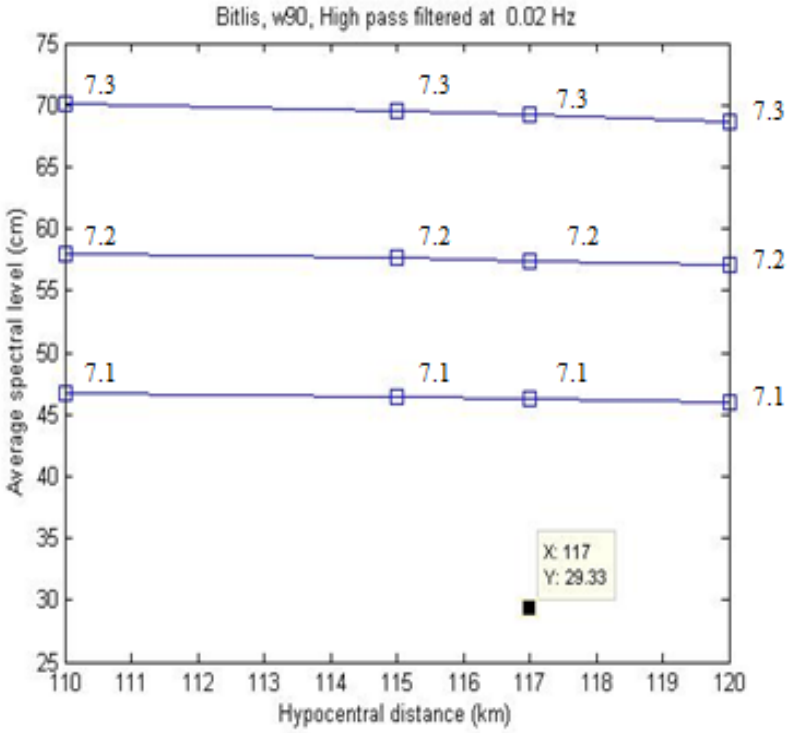

Figure 4.1. For a 90 s time window the real spectral level of strong-motion records at Bitlis station (averages over three components) is shown by a black point.

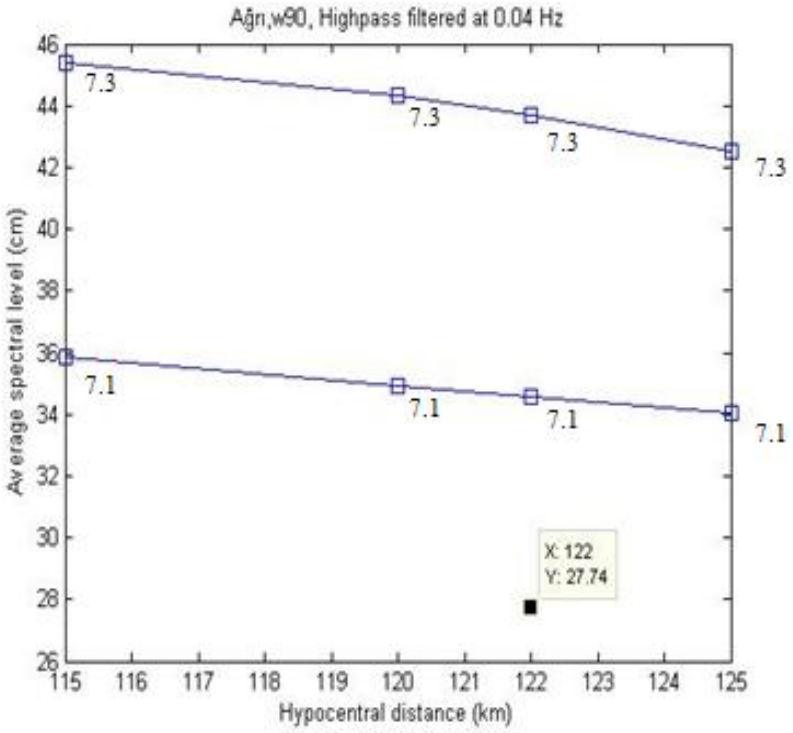

Figure 4.2. For a 90s time window the real spectral level of strong-motion records at Ağrı station (averages over three components) is shown by a black point.

For both stations, M_W value is apparently less than 7.1. For exact computation of M_W we introduce the following Equation (4.1.): Since spectral level scales with moment magnitude, we propose a relationship between spectral level S_L and M_W similar to the relationship between M_0 and M_W (3.3.1).

$$M_W = a \log(S_L) + b \text{ , (Hypocentral distance kept constant)} \quad (4.1)$$

Where S_L is the average spectral level, *a* and *b* are constants to be determined by simple line fitting of the synthetic data. For a given magnitude spectral level decreases with distances, as a result of geometric wave attenuation. We consult this Equation to calculate moment magnitude especially if the real spectral level for a time window is out of the synthetic spectral level range enclosed by $M_W7.1$ – $M_W7.3$. Because we did not prepared the spectral levels for all magnitude values, interpolation is limited.

Example 4.1. Exact Computation of M_W with respect to Bitlis station for 60s time window.

Bitlis station is at 117 km and for 60s time window (w60) we have the following values:

M_W	S_L	$\log(S_L)$
7.1	28.62	1.46
7.2	33.58	1.53
7.3	37.65	1.58

Using the Equation (4.1); we get best values a = 1.65 and b = 4.68 by least square fitting of a line. In our calculations a value is usually positive and greater than 1.

$$M_W = 1.65\log(S_L) + 4.68 \quad (4.2)$$

Finally we determine the moment magnitute for the real spectral level (27.74).

$$M_W = 1.65\log(27.74) + 4.68 \quad (4.3)$$

$$M_W = 7.06,\ M_W \sim 7.1.$$

Performing the same procedure for other time windows we get Table 4.1. and Table 4.2. which includes all M_W values corresponding to different time windows. For time windows shorter than 53 s we made computation with two high-pass frequencies mention in (3.4.2) to see how the selected high-pass frequency affect the results.

Table 4.1. Moment magnitude (M_W) vs Time window(s) for Station Bitlis.

Time window (s)	Moment magnitude (M_W)	High-pass frequency (Hz)
30	9.0	0.25
30	7.4	0.02
40	8.3	0.25
40	7.9	0.02
50	9.8	0.25
50	7.3	0.02
60	7.1	0.02
70	6.8	0.02
80	6.84	0.02
90	6.89	0.02

Table 4.2. Moment magnitude (M_W) vs Time window(s) for Station Ağrı.

Time window (s)	Moment magnitude (M_W)	High-pass frequency (Hz)
30	9.6	0.25
30	8.4	0.04
40	7.8	0.25
40	9.1	0.04
50	7.9	0.25
50	8.8	0.04
60	7.8	0.04
70	7.3	0.04
80	6.94	0.04
90	6.91	0.04

All these values are combined in the following graph showing the behaviour of moment magnitude with time window. For short time windows M_w values resulting in case of high-pass filtering with 0.25 Hz are drawn (Figure 4.3).

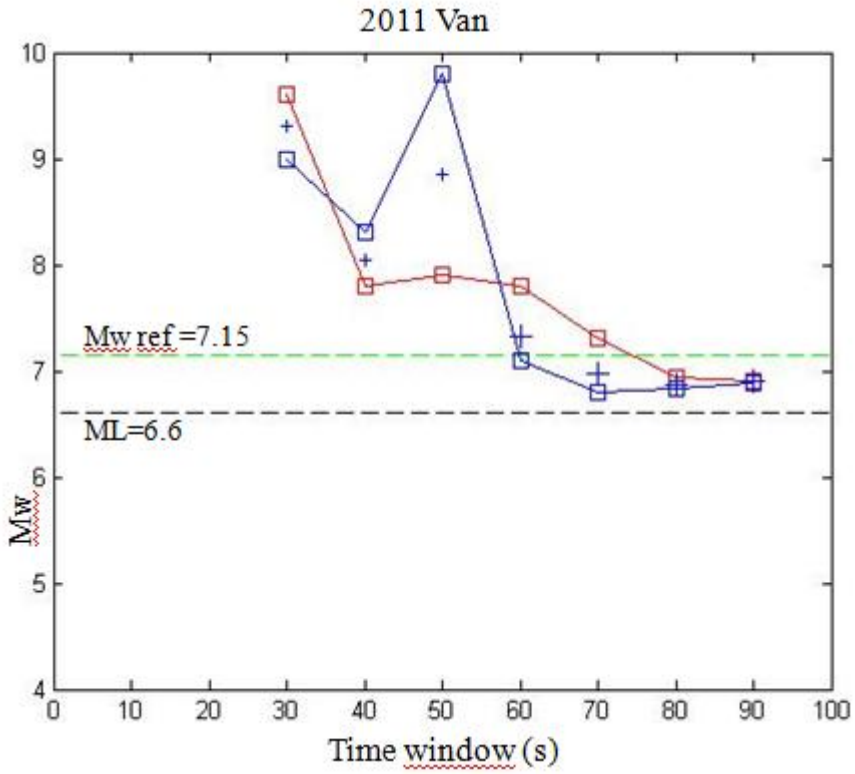

Figure 4.3. Graph showing the evolution of computed MW as a function of time measured from the earthquake origin time (T=0).

Average M_w is obtained by averaging the magnitude values of both stations in the selected time window. A weight is attributed to each individual station depending on the high-pass filtering used (see text Section 3.4.3). The average M_w is represented by a blue plus sign whose size is proportional to the sum of weights. Larger sizes are expected to provide better estimates. Since less than three stations are used, error bars are not drawn. Continuous lines indicate the maximum and minimum values of magnitude found among stations (blue for Bitlis and red for Ağrı). The local magnitude (M_L=6.6) is drawn by dashed black line. And the reference moment magnitude value (M_w ref=7.15) is shown by dashed green line.

The weighted mean values of M_w corresponding to time windows are 9.3, 8.05, 8.85, 7.33, 6.97, 6.87, and 6.9 respectively. Thus we get M_w= 6.9 for 90 s time window. This is the value that can be announced. This result may be improved by doing computations for more stations.

5. DISCUSSION

5.1. Comparison and Validation

One of the main points that needs to be explained is the apparent overestimation of M_W in case of short time windows (30, 40, and 50 s) for which 0.25 Hz high-pass frequency is used. In comparison with previous applications (Delouis *et al*., 2009) we obtained unexpectedly high values of M_W for short time windows. That's why we made computation for these time windows without changing the high-pass frequency that we found out by observing the spectra of accleration as well. As can be seen we still couldn't get better results especially for Ağrı station.

The main reason behind this anomaly is the misalingment of the real displacement seismograms with the corresponding synthetic displacement seismogram. In real seismograms waves arrive about 5 s earlier than in synthetics (Figure 3.6). This means for the same window length real seismograms contains more waves, which increased the real spectral levels relative to the synthetic spectral levels. Secondly, it is observed that synthetic amplitudes are generally smaller (probably because of velocity model) which also contributed to this situation.

This anomaly may also be explained by slip distribution along the rupture plane. Synthetic seismograms are computed by assuming that the slip is constant over the rupture plane. If in the hypocentral area the real slip is higher, we get overestimation of M_W for short time windows, which include waves coming from hypocentral area. After 50 s the value of the moment magnitude approaches to the reference moment magnitude level (M_W=7.15) and for a time window ending 90 s after origin time the average magnitude is 6.9.

Inadequacies of the method are related to the arbitrariness in the definition of the six different focal mechanisms in computing of the synthetic seismograms, the degree of uncertainty in the azimuth of the station, the depth of the hypocenter in the fault models, the rupture propagation, and the 1D crustal model. It is stated in Delouis *et al*. (2009) that a series of sensitivity tests to assess the robustness of the method, varying the model

parameters used to compute the synthetic data. As a result it is found out that the performance of the method could be improved by using a velocity model adapted to each study area.

5.2. Critique of the Method

Although it turns out that the method is confirmed to work for many earthquakes, it needs theoretical explanation. Why is the maximum of the spectral plateau at low frequency (spectral level) scaling with magnitude? The scaling of spectral level with M_W is accepted only by empirical justification over synthetic records.

In cases where the epicentral distances of stations are large enough that they can not be considered to be in the near-field, we expect to compute M_W from the displacement spectrum of body waves (P-wave or S-wave). Because waves appear separately in the seismogram without interferences. And there is theoretical ground of computing seismic moment from the flat part of the spectrum of P-wave at low frequencies (below corner frequency).

However with MWSYNTH method whatever be the epicentral distance of the station the computing of M_W is done by interpolation in the tables of spectral levels for all time windows (windows may include different wave trains). Thus the computation of M_W does not correspond to the well-known way of computation.

The increment in the length of time windows is taken as 10s. This is suitable to observe the behavior of M_W with respect to time window. Because the aim is the fast determination of magnitude we want to see in principle the time when the magnitude value is stabilized first. So large increments cost time (recording time). But using small increments has an important result. If the increment is choosen sufficiently small that the P-wave can be compelety included in a time window *W*, then the M_W value corresponding to *W* is the true value because at this point the computation of magnitude is similar with the well known way of magnitude computation. In the well-known way of magnitude computation we obtain seismic moment from the flat part of the P-wave spectrum and use the Equation (3.1) by Kanamori (1977). That's why the proposal we made in Equation 4.1

should somehow evolve to (3.3.1) for the time window *W*. This is the motivation behind Equation 4.1. Thus by introducing the Equation (4.1) we not only have the possibility of exact computation of magnitude but also bring about some theoretical consideration. We tried to make a generalization of the computation of moment magnitude from the displacement spectrum.

By chance in this application we have the possibility of obtaining magnitude value for a 30 s time window much earlier than 90 s. Because 30 s time window includes P-wave completely. However as can be seen from the results, magnitude value is overestimated for 30 s time window. The possible reasons of this anomaly are explained in Section (5.1). After all, there exist a time window *W* (shortest time window allowing correct theoretical computation of M_W) much earlier than the time of the stabilization of M_W. On the otherhand, since the number of time windows increases, computing may take more time. Thus, 10 s increment may not be the optimal value for rapid estimation of M_W.

Since the Equation 4.1 provides us the opportunity of determining M_W with a few data points from the table of spectral level (at constant distances). It can be used to prepare complete tables of spectral levels easily.

6. CONCLUSION

An agreeable estimation of moment magnitude (M_w =6.9) for the 23 October 2011 Van Earthquake is obtained using strong-motion records. The result is obtained using a time window ending 90 sec after earthquake origin time and with determination of the optimal high-pass frequency.

This study provides a recovery of M_w for the 23 October 2011 Van Earthquake. Thus for the case of Van Earthquake the MWSYNTH method is applicable in the epicentral distances about 120 km. Results may be improved by doing computations for more stations.

The method can be implemented for automated near real-time determination of Mw. It is possible to obtain rapid estimation of moment magnitude within about 100 sec after origin time (recording+computing time).

The time delay may be reduced by using shorter time windows, but in that case an overestimation of M_w (in this application) occur. A delay of one to two minutes may be well adapted for most regional tsunami warning systems. On the other hand, magnitude determination may not be fast enough in cases where early seismic warning is needed to alert target areas located short distances from the recording stations.

REFERENCES

Aki, K. and P. G. Richards, 1980, *Quantitative Seismology,* Vol.1, W. H. Freeman and Co., 512 pp. San Francisco.

Albini, P., M. B. Demircioglu, M. Locati, A. Rovida, K. Şeşetyan, M. Stucchi, and D. Viganò, 2012, "In Search of the Predecessors of the 2011 Van (Turkey) Earthquake", *Seismological Research Letters,* 83, N. 5, pp. 855-862.

Allen, R. M. and H. Kanamori, 2003, "The Potential for Earthquake Early Warning Southern California", *Science* 300, 786–789.

Ambraseys, N. N., 1989, "Temporary Seismic Quiescence: SE Turkey", *Geophys. J. Int,* 96, No. 2, 311–331.

Ambraseys, N. N., 2001, "Reassessment of Earthquakes, 1900–1999, in the East Mediterranean and the Middle East", *Geophys. J. Int.* 145, pp. 471–485.

Ambraseys, N. N., and J. A. Jackson, 1998, "Faulting Associated with Historical and Recent Earthquakes in the Eastern Mediterranean Region", *Geophys. J. Int.* 133,390–406.

Barka, A. and Kadinsky-Cade, 1988, "Strike Slip Fault Geometry in Turkey and its Influence on Earthquake activity", *Tectonics,* 7(3), pp. 663-684.

Barka A.and R.Reilinger, 1997,"Active Tectonics of the Eastern Mediterranean Region: Deduced from GPS, Neotectonic and Seismicity Data", *Ann. Geofis.,* XL13, No. 3, 587-610.

Bolt, B.A., 1978, "The Local Magnitude ML of the Kern County Earthquake of July 21, 1952", *Bull. Seismol. Soc. Am.,* 68, pp. 513-515.

Bouchon, M., 1981, "A Simple Method to Calculate Green's Functions for Elastic Layered Media", *Bull. Seismol. Soc. Am.,* 71, No. 4, 959–971.

Bozkurt, E., 2001, "Neotectonics of Turkey - A Synthesis", *Geodinamica Acta,* No. 14, pp. 3-30.

Brune, J.N., 1970, "Tectonic Stress and The Spectra of Seismic Shear Waves from Earthquakes", *J. Geophys. Res.* 75, No. 26, pp. 4997-5009.

Brune, J.N., 1971, "Correction", *J. Geophys. Res.* 76, No.20, 5002.

Delouis, B., J. Charlety , M. Vallée 2009, "A Method for Rapid Estimation of Moment Magnitude Mw for Moderate to Large Earthquakes from Near-field Spectra of Strong-motion Records (MWSYNTH)", *Bulletin of Seismological Society of America,* 99, No. 3, pp. 1827-1840.

DeMets, C., R.G. Gordon, D.F. Argus, and S. Stein, 1990, "Current Plate Motions",*Geophys. J. Int.* 101, pp. 425-478.

DeMets, C., R.G. Gordon, D.F. Argus, and S. Stein, 1994, "Effects of Recent Revisions to the Geomagnetic Reversal Time Scale on Estimates of Current Plate Motions ", *Geophysical Research Letters,* No. 21, pp. 2191–2194.

Emre O., T.Y. Duman, S. Özalp, H. Elmacı, 2011, "Site Observations and Preliminary Evaluation of Source Fault of 23 October 2011 Van Earthquake". *Active Tectonics Research Group, MTA Publications,* Ankara (in Turkish).

Geller, R.J. and H. Kanamori, 1977, "Magnitudes of Great Shallow Earthquakes from 1904-1952", *Bull. Seismol. Soc. Am.,* No. 67, pp. 587-598.

Guttenberg, B. and C.F. Richter, 1954, *Seismicity of the Earth,* 2nd ed. 310 pp. Princeton University Press, Princeton, N.J.

Hanks T.C. and H. Kanamori, 1979, "A Moment Magnitude Scale" *J. Geophys. Res.*, 84, No. b5, pp. 2348-2350.

Hanks T.C., J.A. Hileman, and W. Thatcher, 1975, "Seismic Moments of the Larger Earthquakes of the Southern California Region", *Geol. Soc. Amer. Bull.*, No. 86, pp. 1131-1139.

Heaton, T.H., 1990, "Evidence for and Implications of Self-healing Pulses of Slip in Earthquake Rupture", *Physics of the Earth and Planetary Interiors*, No. 64, pp. 1-20.

Hileman J.A., C.R. Allen, and J.M. Nordquist, 1973, "Seismicity of the Southern California Region 1 January 1932 to 31 December 1972, Report", Seismol. Lab. Calif. Inst. of Technol. Pasadena.

Jackson, J.A., 1992, "Partitioning of Strike-Slip and Convergent Motion Between Eurasia and Arabia in Eastern Turkey and the Caucasus", *J. Geophys. Res.* Vol. 97, No. b9, pages 12,471-12,479.

Jackson, J.A. and D. McKenzie, 1988, "The Relationship Between Plate Motions and Seismic Moment Tensors, and The Rates of Active Deformation in The Mediterranean and Middle East", *Geophys. J. R. astr. Soc*,. 93, 45-73.

Kanamori, H., 1977, "The Energy Release in Great Earthquakes", *J. Geophys. Res.*, 82, No. 20, pp. 2981-2987.

Kanamori, H. and D.L. Anderson, 1975, "Theoretical Basis of Some Empirical Relations in Seismology", *Bulletin of the Seismological Society of America.* 65, No. 5, pp. 1073-1095.

Kanamori, H. and P.C. Jennings, 1978, "Determination of Local Magnıtude, M_L, from Strong- motion Accelerograms", *Bulletin of Seismological Society of America*, No. 68, 2, pp. 471-485.

Koçyiğit, A., A. Yılmaz, S. Adamia and S. Kuloshvili, 2001, "Neotectonics of East Anatolian Plateau (Turkey) and Lesser Caucasus: Implication for Transition from Thrusting to Strike-Slip Faulting", *Geodinamica Acta,* No. 14, pp. 177-195.

Lay, T. and T.C. Wallace, 1995, *Modern Global Seismology,* Elsevier Science.

Lundgren, P., D. Giardini, and R. Russo, 1998, " A Geodynamic Framework for Eastern Mediterranean Kinematics", *Geophy. Res. Lett.,* 25, 4007 –4010.

McClusky, S., S. Balassanian, A. Barka, C. Demir, S. Ergintav, L. Georgiev, O., Gurkan, M. Hamburger, K. Hurst, H. Kahle, K., Kastens, G. Kekelidze, R. King, V. Kotzev, O. Lenk, S. Mahmoud, A. Mishin, M. Nadariya, A. Ouzounis, D. Paradissis, Y. Peter, M. Prilepin, R. Reilinger, I. Sanli, H. Seeger, A. Tealeb, M.N. Toksöz and G. Veis, 2000, "Global Positioning System Constraints on Plate Kinematics and Dynamics in the Eastern Mediterranean and Caucasus", *Journal of Geophysical Research: Solid Earth,* No. 105, pp. 5695-5719.

McKenzie, D., 1972, "Active Tectonics of Mediterranean Region", *Geophysical Journal of the Royal Astronomical Society,* No. 30, pp. 109-185.

Örgülü, G., M. Aktar, N. Türkelli, E. Sandvol, M. Barazangi, 2003, "Contribution to the Seismotectonics of Eastern Turkey from Moderate and Small Size Events", *Geophysical Research Letters,* No. 30, pp. 24.

Reilinger, R., S. McClusky, P. Vernant, S. Lawrence, S. Ergintav, R. Cakmak, H. Ozener, F. Kadirov, I. Guliev, R. Stepanyan, M. Nadariya, G. Hahubia, S. Mahmoud, K.Sakr, K., A. ArRajehi, D. Paradissis, A. Al-Aydrus, M. Prilepin, T. Guseva, E. Evren, A. Dmitrotsa, S.V. Filikov, F. Gomez, R. Al-Ghazzi and G. Karam, 2006,"GPS Constraints on Continental Deformation in the Africa-Arabia-Eurasia Continental Collision Zone and Implications for the Dynamics of Plate Interactions", *Journal of Geophysical Research-Solid Earth,* B05411, pp. 1-26.

Reilinger, R.E., S.C. McClusky, M.B. Oral, R.W. King, M.N. Toksoz, A.A. Barka, I. Kinik, O. Lenk, and I. Sanli, *1997*, "Global Positioning System Measurements of Present-day Crustal Movements in the Arabia-Africa-Eurasia Plate Collision Zone", *J. Geophys. Res.*, No. 102, pp. 9983-9999.

Shebalin, N. V., and R. E. Tatevossian, 1997, "Catalogue of Large Historical Earthquakes of the Caucasus, in Historical and Prehistorical Earth-quakes in the Caucasus", *Kluwer Academic Publishing, Dordrecht,* Netherlands, pp. 201–232.

Soysal H., S. Sipahioglu, D. Kolcak, and Y. Altinok, 1981, "Türkiye ve Çevresinin Tarihsel Deprem Kataloğu", *TUBITAK,* Proje no. TBAG 341, Istanbul, 86 pp.

Sato, R., 1989, "Handbook of Fault Parameters for Japanese Earthquakes", Kajima Institute Publishing Co. Ltd., Tokyo (in Japanese).

Şaroğlu, F. and Y. Güner, 1981, "Doğu Anadolu'nun Jeomorfolojik Gelişimine Etki Eden Öğeler: Jeomorfoloji, Tektonik, Volkanizma İlişkileri", *TJK Bull.,* No. 24, pp. 39-50.

Şengör, A.M.C., S. Özeren, T. Genç and E. Zor, 2003, "East Anatolian High Plateau as a Mantle-Supported, North-South Shortened Domal Structure", *Geophysical Research Letters,* No. 30, pp. 8045.

Taşkın, B., A. Sezen, U.M. Tuğsal and A. Erken, 2013, "The Aftermath of 2011 Van Earthquakes: Evaluation of Strong Motion, Geotechnical and Structural Issues", *Bulletin of Earthquake Engineering*, No. 11, pp. 285-312.

Tchalenko, J. S., 1977, "A Reconnaissance of The Seismicity and Tectonicsat The Northern Border of The Arabian Plate (Lake Van Region) ", *Revue de Géographie Physique et Geólogie Dynamique,* No. 19, pp. 189–208.

Thatcher W. and T.C. Hanks, 1973, "Source Paremeters of Southern California Earthquakes", *J. Geophys. Res.* No. 78, pp. 8547-8576.

Trifunac, M.D. and J.N. Brune, 1970, "Complexity of Energy Release During the Imperial Valley, California, Earthquake of 1940", *Bull. Seismol. Soc. Am.,* No 60, pp.137-160.

Wells, D. L. and K. J. Coppersmith, 1994, "New Empirical Relationshipsamong Magnitude, Rupture Length, Rupture Width, Rupture Area, and Surface Displacement", *Bull Seismol. Soc. Am.*No 84, pp. 974–1002.

Wu, Y.-M. and H. Kanamori, 2008, "Development of an Earthquake Early Warning System Using Real-time Strong-motion Signals", *Sensors* 8, 1–9.

Wu, Y.-M., and L. Zhao, 2006, "Magnitude Estimation Using the First Three Seconds P-Wave Amplitude in Earthquake Early Warning", *Geophys. Res. Lett.* L16312, doi 10.1029/2006GL026871.

Wu, Y.-M. and T. L. Teng, 2004, "Near Real-time Magnitude Determination for Large Crustal Earthquakes", *Tectonophysics,* No. 390, pp. 205–216.

Yeh, H.-C., 1975, *Mechanism of the 1927 Lompoc Earthquake from Surface Wave Analysis*, M.S. Thesis, Univ. of Washington, Seattle.

Yorihiko, O., 1976, *Spectral Analysis of Earthquake Wave*, Kajima Institute Publishing Co., Ltd. (Turkish translation).

Zhu L., 2011, "Synthetic Seismograms and Seismic Waveform Modeling", Saint Louis University.

Zollo, A., M. Lancieri, and S. Nielsen, 2006, "Earthquake Magnitude Estimation from Peak Amplitudes of Very Early Seismic Signals on Strong-motion Records", *Geophys. Res. Lett.* 33, L23312, doi 10.1029/2006GL027795.

DATA SOURCES

AFAD (http://kyh.deprem.gov.tr/ftpe.htm)

APPENDIX A. STRONG GROUND MOTION RECORDS OF TURKEY

PLACE : BİTLİS MERKEZ DSİ 173. ŞUBE

EARTHQUAKE DATE : 2011/10/23 10:41:20 (GMT)

EPICENTER COORDINATES : 38.68900N-43.46570E

EARTHQUAKE DEPTH (km) : 19.02

EARTHQUAKE MAGNITUDE : 6.7 ML

STATION ID : 1302

STATION COORDINATES : 38.47440N-42.15913E

STATION ALTITUDE (m) :

RECORDER TYPE : Guralp cmg5td

RECORDER SERIAL NO : T5J60/A1032

RECORD TIME : 23/10/2011 10:41:18.000000 (GMT)

NUMBER OF DATA : 19107

SAMPLING INTERVAL (sec) : 0.01

RAW PGA VALUES (cm/s^2) : (N-S) 89.668149 (E-W) 102.243526 (U-D) 35.511623

PLACE : AĞRI MERKEZ BAYINDIRLIK VE İSKAN MÜDÜRLÜĞÜ

EARTHQUAKE DATE : 2011/10/23 10:41:20 (GMT)

EPICENTER COORDINATES : 38.68900N-43.46570E

EARTHQUAKE DEPTH (km) : 19.02

EARTHQUAKE MAGNITUDE : 6.7 ML

STATION ID : 0401

STATION COORDINATES : 39.71978N-43.01640E

STATION ALTITUDE (m) : 1647

RECORDER TYPE : Guralp cmg5td

RECORDER SERIAL NO : 5D60

RECORD TIME : 23/10/2011 10:40:43.000000 (GMT)

NUMBER OF DATA : 22241

SAMPLING INTERVAL (sec) : 0.01

RAW PGA VALUES (cm/s^2) : (N-S) 18.459245 (E-W) 15.087845 (U-D) 7.2174

APPENDIX B. CODES PREPARED FOR CALCULATIONS AND DATA PROCESSING

1. CALCULATION OF HYPOCENTRAL DISTANCE IN MATLAB

As an example the calculation of the hypocentral distance for Bitlis station is shown below.

```
arclen=distance('gc',[38.68900,43.46570],[38.47440,42.15913]);% Geographic coordinates
% of Bitlis station and that of the Earthquake epicentre. This gives the epicentral distance
%  (angle) in degree.
delta=arclen*2*pi/360; % in radian
R=earthRadius;
l=R*sqrt(2*(1-cos(delta))); % epicentral distance in meters
d=19020; % depth of hypocentre in meters
alfa=(pi-delta)/2;
h=sqrt(l^2+d^2-2*l*d*cos(alfa)); % hypocentral distance in meters
```

2. CALCULATION OF AZIMUTH IN MATLAB

Epicenter coordinates : 38.68900N-43.46570E

Bitlis station coordinates : 38.47440N-42.15913E

Ağrı station coordınates : 39.71978N-43.01640E

(http://kyh.deprem.gov.tr/ftpe.htm)

```
az = azimuth('rh',38.68900,43.46570,38.47440,42.15913)
```

az=258° (Bitlis)

```
az = azimuth('rh',38.68900,43.46570,39.71978,43.01640)
```

az=341° (Ağrı)

(For azimuth determination scheme see modern global seismology p.340)

3. DATA PROCESSING IN MATLAB

```
%baseline correction
A=load('20111023104120_1302.txt'); % Bitlis station uncorrected record.
A3=A(:,3); % vertical component
dt=0.01; % sampling interval in sec
%origin time=10:41:20 (GMT)
%record time=10:41:18 (GMT)
Vpmax=6.4; % upper limit for P-wave velocity in km/sec
Vpmin=5.6; % lower limit for P-wave velocity in km/sec
Tpmin=(h*1/10^3)/Vpmax
Tpmax=(h*1/10^3)/Vpmin
% travel time( difference between
% -arrival time and origin time)
Vsmin=(3/5)*Vpmin;
Vsmax=(3/5)*Vpmax;
Tsmax=(h*1/10^3)/Vsmin;
Tsmin=(h*1/10^3)/Vsmax;
Ts=(Tsmin+Tsmax)/2;

B3=A3(2/dt+1,1); % record from the origin time
for i=2/dt+2:length(A)
   B3=[B3;A3(i,1)];
End
H=abs(B3);
for i=2:length(B3)-1
   if H(i,1)>H(i-1,1) & H(i,1)>H(i+1,1)
      P(i,1)=H(i,1);
   else
      P(i,1)=0;
   end
end
```

```
Nmin=round(Tpmin/dt+1);
Nmax=round(Tpmax/dt+1);

for i=1:Nmin
   s(i,1)=P(i,1);
end

x(1,1)=1;
for i=2:Nmin
   if s(i,1)==0
      x(i,1)=x(i-1,1)+1;
   else
      x(i,1)=x(i-1,1);
   end
end

mean_peak=sum(s)/(Nmin-max(x));% mean of non-zero values of P until Nmin.
for j=Nmin+1:length(H)
   if H(j,1)>3*mean_peak
   S(j,1)=1;
   else
   S(j,1)=0;
   end
end

for k=length(S):-1:1
    if S(k,1)==1
       Np=k;
    end
 end

Tp=(Np-1)*dt; % P-wave arrival time
for i=1:Np-(3/dt+1)
```

```
   b(i,1)=B3(i,1);
end
mean=sum(b)/length(b); % average amplitude of the pre-event noise from origion time to 3
% seconds preceding the first P-arrival)
for i=1:length(B3)
   newB3(i,1)=B3(i,1)-mean;
end
% newB3 is acceleration after the simple correction.
% we will do essential corrections from now on.
% the following operation (Wu&Teng method) is done if there are late arrivals in the
% displacement seismogram obtained from newB3.
M=abs(newB3);
h=max(M)/5
for j=1:length(B3)
   if M(j,1)==max(M)
     m=j;
   end
end

a=1;
for k=m+1:length(B3)
   if M(k,1)>=h
     a=[a;1];
     elseif M(k,1)<h
          a=[a;0];
   end
end

for i=1:length(a)
   if a(i,1)==0
     c(i,1)=c(i-1,1)+1;
     elseif a(i,1)==1
          c(i,1)=0;
```

```
    end
end

N=round(5/dt+1);
c1=0;
for i=2:length(a)
    if c(i,1)==N
       c1=[c1;1];
    else
       c1=[c1;0];
    end
end

for r=length(a):-1:1
    if c1(r,1)==1
       n=r;
    end
end

% so the length of data is m+n-1
Te=(m+n-2)*dt; % End of event time of the strong-shaking duration

for i=1:length(B3)
    if i<=m+n-1
        a3(i,1)=newB3(i,1);
    else
        a3(i,1)=0;
    end
end
%if there is no late arrivals in the displacement record then no need toapply Wu&Teng
%method.(we replace newB3 by a3). In the case of late arrivalse a3 is the acceleration
%record.% for further processing we look at acceleration spectrumthat is the spectrum of
newB3 or % that of a3.
```

4. CALCULATION OF DISPLACEMENT SPECTRUM IN MATLAB

```
A=data;% As an example the vertical component of acceleration data for a 80s time
% window at Bitlis station is choosen
dt=0.01;% sampling interval
fs=1/dt;% sampling frequency or rate
fn=fs/2;% nyquist frequency
%velocity and displacement
V=cumtrapz(A)*dt;
D=cumtrapz(V)*dt;
[b,a] = butter(4,0.02/fn,'high'); % we determined 0.02 Hz from the V-shaped
% acceleration spectrum.we use it for windows which include S-wave+20 sec.
% for shorther windows we use 0.25 Hz
x=filter(b,a,D);% filtered displacement seismogram.
Fs=100;
L=length(x);
NFFT = 2^nextpow2(L); % Next power of 2 from length of y
Y = fft(x,NFFT)*dt;
f = Fs/2*linspace(0,1,NFFT/2+1);
% Plot single-sided amplitude spectrum.
loglog(f,abs(Y(1:NFFT/2+1)))
title('Displacement Spectrum of Bitlis U-D w80')
xlabel('Frequency (Hz)')
ylabel('Displacement spectrum (cm.sec)')
```

5. COMMANDS FOR GENERATION OF GREEN'S FUNCTIONS AND SYNTHETIC WAVEFORMS

For Green's functions:

./fk.pl –Mmodel/depth[/f] [-Nnt/dt/smth/dk/taper] –D

-model (velocity model)

-depth (centroid dept)

-nt (total number of points, 2^n)

-dt (sampling rate)

-smth (interpolation option)

-dk (infinitesimal grid size)

-D (distances)

For senthetic waveforms:

./syn -M(d|f)mag/Strike/Dip/Rake [-SsrcFunctionName | -Ddura/rise] [-I] -Aazimuth -OoutName –GfirstCompOfGreen

-A azimuth

-D specify the source time function as a trapezoid, give total duration and rise-time point (0-0.5) (rupture time)

-G the name of the first component of the Green's function-I integration once (for displacement)

-Md double-couple source-Mf single force source-O output file name -P compute static displacement, input greens from stdin

-S input the SAC file name of the source time function

APPENDIX C. DETERMINATION OF HIGH-PASS FREQUENCY FROM THE ACCELERATION SPECTRUM

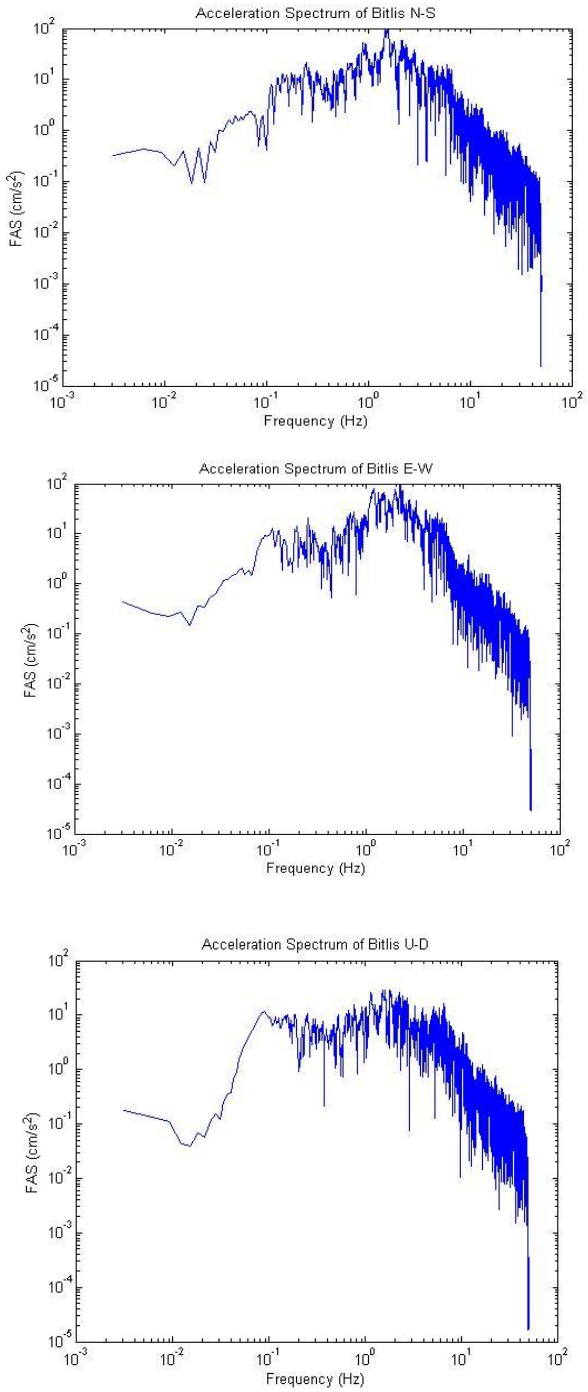

Figure C.1. Acceleration spectra for three components of Bitlis station. Approximate high-pass frequencies for N-S, E-W and U-D components are 0.02 Hz, 0.015 Hz, and 0.015 Hz respectively. The highest value is 0.02 Hz.

As for the Ağrı station;

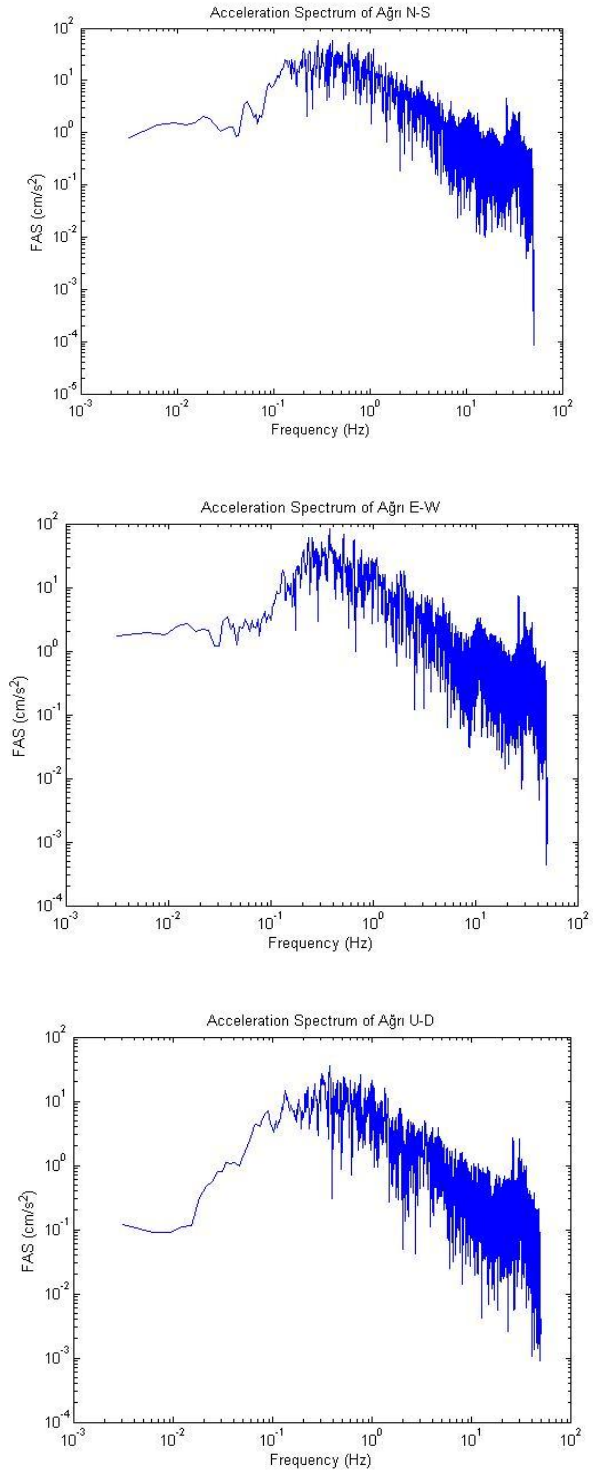

Figure C.2. Acceleration spectra for three components of Ağrı station. Approximate high-pass frequencies for N-S, E-W and U-D components are 0.04 Hz, 0.03 Hz, and 0.009 Hz respectively. The highest value is 0.04 Hz.

APPENDIX D. LIST OF SPECTRAL LEVELS OF REAL AND SYNTHETIC RECORDS

Table D.1. List of Real Spectral Levels

For time windows shorter than 53s, spectral levels are computed for two high-pass frequencies.

Station : Bitlis

Hypocentral distance =117 km

		Spectral levels (cm.sec)			
Window(s)	High-pass frequency(Hz)	NS	EW	UD	Average
90	0.02	20.13	28.05	39.35	29.33
80	0.02	20.20	28.21	38.73	29.05
70	0.02	19.55	28.34	36.64	28.00
60	0.02	18.36	28.27	36.60	27.74
50	0.25	1.56	1.35	1.09	1.34
50	0.02	13.39	18.68	25.01	19.02
40	0.25	0.53	0.92	0.48	0.64
40	0.02	5.77	10.08	7.02	7.62
30	0.25	0.11	0.29	0.13	0.18
30	0.02	0.71	1.71	0.78	1.67

Station : Ağrı

Hypocentral distance = 122 km

		Spectral levels (cm.sec)			
Window(s)	High-pass frequency(Hz)	NS	EW	UD	Average
90	0.04	34.63	24.81	23.77	27.74
80	0.04	33.04	25.94	22.68	27.22
70	0.04	32.97	22.89	26.74	27.54
60	0.04	30.21	17.93	22.92	23.68
50	0.25	1.45	1.78	1.23	1.49
50	0.04	21.01	14.71	17.92	17.88
40	0.25	0.53	0.76	0.62	0.63
40	0.04	13.94	7.67	7.08	9.56
30	0.25	0.19	0.33	0.44	0.32
30	0.04	2.39	2.38	2.09	2.29

Table D.2. List of Synthetic Spectral Levels

Bitlis station

Hypocentral distance = 117 km

Mw	window (sec)	Distance (km)	average spectral level (cm.sec)	
7.1	30	110	0.0150	
		115	0.0128	
		117	0.0129 (0.25 Hz)	1.1601 (0.02 Hz)
		120	0.0123	
7.1	40	110	0.0777	
		115	0.0625	
		117	0.0559 (0.25 Hz)	4.0477 (0.02 Hz)
		120	0.0440	
7.1	50	110	0.2311	
		115	0.1993	
		117	0.1913 (0.25 Hz)	12.9676 (0.02 Hz)
		120	0.1692	
7.1	60	110	32.0555	
		115	29.6947	
		117	28.6166	
		120	26.8250	
7.1	70	110	45.3071	
		115	43.3089	
		117	42.1393	
		120	39.8301	

7.1	80	110	47.2334
		115	46.3557
		117	45.9390
		120	45.2111
7.1	90	110	46.7364
		115	46.3891
		117	46.2055
		120	45.9066

Mw	window (sec)	Distance (km)	average spectral level (cm.sec)
7.2	30	110	0.0192
		115	0.0167
		117	0.0154
		120	0.0138
7.2	40	110	0.1090
		115	0.0871
		117	0.0788
		120	0.0615
7.2	50	110	0.2317
		115	0.2129
		117	0.2047
		120	0.1748
7.2	60	110	37.7460
		115	34.8309
		117	33.5801
		120	31.4457

7.2	70	110	53.7688	
		115	49.9839	
		117	48.1521	
		120	45.0105	
7.2	80	110	57.7033	
		115	56.1407	
		117	55.4464	
		120	54.3057	
7.2	90	110	58.0263	
		115	57.6197	
		117	57.4196	
		120	57.0815	

Mw	window (sec)	Distance (km)	average spectral level (cm.sec)	
7.3	30	110	0.0214	
		115	0.0187	
		117	0.0173 (0.25 Hz)	1.4728 (0.02 Hz)
		120	0.0156	
7.3	40	110	0.0929	
		115	0.0863	
		117	0.0834 (0.25 Hz)	4.8358 (0.02 Hz)
		120	0.0711	
7.3	50	110	0.2118	
		115	0.1784	
		117	0.1560 (0.25 Hz)	18.4006 (0.02 Hz)
		120	0.1445	

7.3	60	110	42.7842
		115	39.2736
		117	37.6472
		120	34.7401
7.3	70	110	60.2409
		115	54.7169
		117	52.4273
		120	48.9707
7.3	80	110	67.5108
		115	65.2178
		117	64.3664
		120	63.1219
7.3	90	110	70.0999
		115	69.5594
		117	69.2335
		120	68.6416

Ağrı station

Hypocentral distance = 122 km

Mw	window (sec)	Distance (km)	average spectral level (cm.sec)	
7.1	30	115	0.0147	
		120	0.0141	
		122	0.0139 (0.25 Hz)	0.4127 (0.04 Hz)
		125	0.0127	
7.1	40	115	0.0664	
		120	0.0475	
		122	0.0415 (0.25 Hz)	1.9277 (0.04 Hz)
		125	0.0382	
7.1	50	115	0.2004	
		120	0.1679	
		122	0.1519 (0.25 Hz)	5.5190 (0.04 Hz)
		125	0.1299	
7.1	60	115	16.1509	
		120	13.3939	
		122	12.5858	
		125	11.6261	
7.1	70	115	25.8830	
		120	23.9122	
		122	23.8451	
		125	22.2400	
7.1	80	115	33.2482	
		120	31.7792	
		122	31.4382	
		125	30.9036	

7.1	90	115	35.8263	
		120	34.8933	
		122	34.5485	
		125	34.0542	

Mw	window (sec)	Distance (km)	average spectral level (cm.sec)	
7.3	30	115	0.0215	
		120	0.0179	
		122	0.0177 (0.25 Hz)	0.5233 (0.04 Hz)
		125	0.0161	
7.3	40	115	0.0899	
		120	0.0762	
		122	0.0658 (0.25 Hz)	2.3054 (0.04 Hz)
		125	0.0556	
7.3	50	115	0.1784	
		120	0.1463	
		122	0.1692 (0.25 Hz)	6.2461 (0.04 Hz)
		125	0.1388	
7.3	60	115	17.3572	
		120	15.6339	
		122	15.1999	
		125	15.1356	
7.3	70	115	30.3036	
		120	28.5892	
		122	27.8110	
		125	26.4370	

7.3	80	115	40.8709
		120	39.5876
		122	38.7774
		125	37.1923
7.3	90	115	45.4066
		120	44.3376
		122	43.7093
		125	42.5383